AN INQUIRY INTO THE APPLICABILITY OF KANTOROVICH'S APPROACH TO THE THERMODYNAMIC OPTIMIZATION

AN INQUIRY INTO THE APPLICABILITY OF KANTOROVICH'S APPROACH TO THE THERMODYNAMIC OPTIMIZATION

BY CONG DAI, B. ENG.

A Thesis Submitted to the School of Graduate Studies in Partial Fulfillment of the
Requirements for the Degree Master of Applied Science

McMaster University

Master of Applied Science (2013) McMaster University

(Engineering) Hamilton, Ontario

TITLE: An inquiry into the applicability of Kantorovich's approach to the thermodynamic optimization

AUTHOR: Cong Dai, B. Eng. (Central South University)

SUPERVISOR: Professor Dmitri V. Malakhov

NUMBER OF PAGES: xiv, 113

ABSTRACT

The purpose of this research has been to reassess the Ag-Mg system using the CALPHAD technique. Compared with previous assessments, we carry out the optimization by fitting calculations to the original data instead of second-hand information. Moreover, we use a two sub-lattice model and a four sub-lattice model based on compound energy formalism to simulate both first-order and second-order transformations between the FCC phase and the $L1_2$ phase. Undoubtedly, the CALPHAD technique has achieved a degree of maturity, but its deficiencies are regularly ignored.

In this thesis, we develop an interval method based on Kantorovich's idea to overcome the shortcomings of the CALPHAD technique. Both advantages and disadvantages of the interval method are discussed. We also present an example of the interval approach on thermodynamic optimization of the Ag-Mg melt. The results suggest that this method would be helpful as a pre-optimization tool.

ACKNOWLEDGEMENTS

I would like to express my deeply felt thanks to my supervisor Dr. Dmitri V. Malakhov for his warm encouragement and thoughtful guidance. His academic attitude and teaching style have impressed me throughout our many fruitful discussions.

I am very grateful to Dr. Gylnis de Silveria, Dr. Nikolas Provatas and Dr. Joseph R. McDermid, who were my lecture supervisors in my first academic year. I am particularly grateful to Dr. Nikolas Provatas for his constant support and valuable suggestions.

Many thanks to Dr. Tony Petric, Dr. Yves Brechet and Dr. James F. Britten for their excellent supervision in my second academic year. I learned a lot from them and am very grateful for discussions with them.

I would like to express my heartfelt gratitude to Mr. Ed. McCaffery, Mr. Doug Culley and Mr. Xiaogang Li, who gave me support in both computational and experimental techniques.

I am also grateful to Mrs. Mah, Mrs. Cole and Mrs. Maltese for their patience and kindness whenever I needed their assistance.

I feel very fortunate to have many friends at McMaster University. Even though we come from different cultures, we have supported each other to share happiness and sadness.

As an international student living far away from home, I am very grateful to my parents for their care and love. Their continuous support let me know that I have the strength to move forward during my toughest times.

LIST OF FIGURES

LIST OF TABLES

SYMBOLS AND ABBREVIATIONS

a_i	Activity of a component *i*
A_i, B_i	Interaction parameters
${}^{\theta}\vec{C}$	Interaction parameters of θ phase
$C(n,m)$	The number of combinations of equations
G_{m}^{θ}	Molar Gibbs energy of θ phase
G_i^{θ}	Partial Gibbs energy of θ phase
$H_{\mathrm{mix}}^{\theta}$	Mixing enthalpy of θ phase
${}^{v}L_{\mathrm{constituents}}^{\theta}$	*v*th order interaction parameter of θ phase between constituents in a sub-lattice
P	Pressure
R	Gas constant (8.31451 J/mol/K)
s	Order parameter
T	Temperature
μ_i^{θ}	Chemical potential of a component *i* in θ phase
w	Statistical weight
x_i^{θ}	Mole fraction of a component *i* in θ phase
y_i^{j}	Site fraction of a component *i* in the *j*th sub-lattice site
ε	Statistical uncertainty
σ	Overall uncertainty

$\forall$	For all, for any
$\exists$	There exists
$\mathrm{A} \in B$	A is an element of the set *B*

1. Introduction

Steels with low composition of inclusions are popularly termed 'Clean Steels', which is a topic of such great industrial interest. There are many studies focusing on the control of inclusions in the production of steel [1-7]. One of the prominent inclusions is $\mathrm{MgO \cdot Al_2O_3}$ spinel, a refractory material that has been researched in several significant publications [3,8-11]. These papers [6,7] suggested that the amount of $\mathrm{MgO \cdot Al_2O_3}$ can be reduced by changing the activity of Mg in molten steel, implying that controlling such a thermodynamic property is crucial to develop clean steels. Based on the Ag-Fe partition technique, Gran *et al*. [12] proposed that the activity of Mg in the Fe-Mg system can be evaluated by measuring the activity of Mg in the Ag-Mg system. For greater details on the Ag-Fe partition technique, see refs. [13-15].

In order to compute such properties, we need to know the Gibbs energies of all the phases involved in the system as they can be used to derive various thermodynamic properties. Therefore, this thesis aims at performing a thermodynamic optimization of the Ag-Mg system. The principal objective of such an optimization is to determine the dependence of molar Gibbs energy of its phase on temperature, pressure and, in the case of solutions, composition.

For a binary ideal solution α at 1 atm, its Gibbs energy can be described as:

$$G^{\alpha}(x_2,T)=(1-x_2)\Delta G_1^{RS(1)\rightarrow\alpha}(T)+x_2\Delta G_2^{RS(2)\rightarrow\alpha}(T)+\underbrace{RT\left[\left(1-x_2\right)\ln\left(1-x_2\right)+x_2\ln x_2\right]}_{\Delta^{\text{ideal}}G},\quad(1.1)$$

where $\Delta G_i^{RS(i)\rightarrow\alpha}$ (i=1, 2) is defined as lattice stability that is equal to the difference of Gibbs energies between each component's reference state (*RS*) and the phase α . It is crucial that the database of lattice stabilities be widely accepted [16,17]. In most situations, the solution is non-ideal, and an excess term would be introduced to reflect the interactions between atoms. As a simple illustration, let us examine the case where the phase α is a regular solution with a temperature-dependent interaction parameter:

$$G^{\alpha}(x_2,T)=(1-x_2)\Delta G_1^{RS(1)\rightarrow\alpha}(T)+x_2\Delta G_2^{RS(2)\rightarrow\alpha}(T)+\Delta^{\text{ideal}}G+\underbrace{x_2(1-x_2)(A+B\times T)}_{\Delta^{\text{excess}}G},\quad(1.2)$$

where A and B are parameters to be determined in order to obtain the value of the Gibbs energy. The most popular method to calculate these parameters is the CALPHAD (CALculation of PHAse Diagram) technique. Since it was proposed in the early 1970s, this technique has enjoyed increasing popularity and has become a successful and widely applied tool in many areas of materials development [18]. This method is based on the utilization of the least squares method to calculate parameters of the Gibbs energy model, and it makes use of all available information about the system because the Gibbs energy model can be derived into many thermodynamic properties. Here is an example to illustrate the technique of CALPHAD:

$$\begin{aligned}&\underbrace{\sum_{i=1}^{l}\omega_i^{{}^{\mathrm{L}}H}\left({}^{\mathrm{L}}H_i^{\exp}-{}^{\mathrm{L}}H^{\mathrm{calc}}\left(x_{2_i},T_i,{}^{\mathrm{L}}\vec{\mathrm{C}}\right)\right)^2}_{\text{Experiment 1}}+\underbrace{\sum_{j=1}^{m}\omega_j^{{}^{\beta}\mu_2}\left({}^{\beta}\mu_{2_j}^{\exp}-{}^{\beta}\mu_2^{\mathrm{calc}}\left(x_{2_j},T_j,{}^{\beta}\vec{\mathrm{C}}\right)\right)^2}_{\text{Experiment 2}}\\&+\underbrace{\sum_{k=1}^{n}\omega_k^{T}\left(T_k^{\exp}-T^{\mathrm{calc}}\left(x_{2_k},T_k,{}^{\mathrm{L}}\vec{\mathrm{C}},{}^{\beta}\vec{\mathrm{C}}\right)\right)^2}_{\text{Experiment 3}}\rightarrow\min\left({}^{\mathrm{L}}\vec{\mathrm{C}},{}^{\beta}\vec{\mathrm{C}}\right),\end{aligned}\tag{1.3}$$

where l, m and n are the numbers of experimental data for experiments 1, 2 and 3 respectively. Experiment 1 is a measurement of the mixing enthalpies in the liquid phase, experiment 2 is a measurement of the chemical potential of the second component in the β phase, and finally experiment 3 is a measurement of the temperature on the liquidus. In addition, $\omega_i^{{}^{\mathrm{L}}H}$, $\omega_j^{{}^{\beta}\mu_2}$ and ω_k^{T} are statistical weights that are calculated by a combination of uncertainties from both experimental observations and conditions in a manner of uncertainty propagation (more details about the uncertainty propagation will be presented in the next chapter). Thus, the CALPHAD technique tries to calculate the best values of the parameters (${}^{\mathrm{L}}\vec{\mathrm{C}}$ and ${}^{\beta}\vec{\mathrm{C}}$) by minimizing the weighted sum of squared differences between experimental and calculated values.

To summarize, the first part of the thesis employ the CALPHAD technique to re-assess the Ag-Mg system. A complete literature review up to 2012 of the Ag-Mg system is presented in Chapter 2, where uncertainty analysis is discussed. Then, based on a good understanding of physical and chemical properties of this system, we formulate the Gibbs energies of all phases, and this modeling procedure is discussed in Chapter 3. Chapter 4 presents the results on comparison with experiments interpreted with statistical and thermodynamic viewpoints. Further, after discussing the statistical disadvantages of the CALPHAD technique in Chapter 5, we introduce an interval approach based on Kantorovich's idea for thermodynamic optimization in Chapter 6 where both advantages and deficiencies of the method are described. Finally, a real thermodynamic optimization by applying the interval approach and its future applications is presented in Chapter 7.

2. Literature review of the Ag-Mg system

2.1. The importance of checking data from original literature

The quality of experimental data plays a significant role in thermodynamic optimization. It is pointless to develop a Gibbs energy model if the selected data are far from their real values. The reasons for bad quality experimental data may come from poor sample preparation, human error and second-hand information. As optimizers, we cannot correct the first two situations, but we should pay more attention whenever using second-hand data. Such information can only be trusted if it is consistent with the original source.

We have found more than 30 papers regarding the Ag-Mg system, and two of them should be first noted. A complete literature review up to 1984 has been presented in the paper by Nayeb-Hashemi *et al.* [19], and Figure 2-1 shows the phase diagram with selected experimental data.

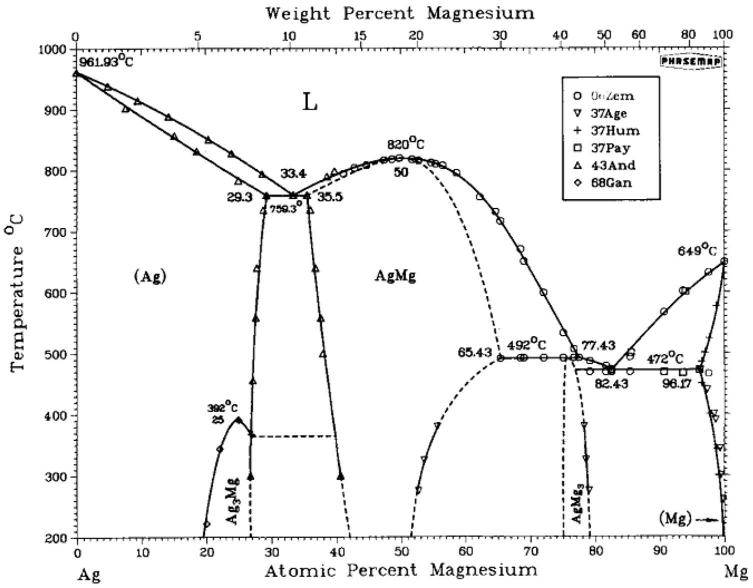

Figure 2-1: Assessed Ag-Mg phase diagram by Nayeb-Hashemi *et al.* [19]

Nevertheless, due to unfathomable reasons, enthalpies of mixing measured by Kawakami [20] were favorably biased according to their report [19]. Since 1984, new experimental data have been made available, and the modeling technique has been improved. Lim *et al.* [21] used literature data and their own calorimetric measurements to build a thermodynamic optimization of this system and the calculated phase diagram is shown in Figure 2-2.

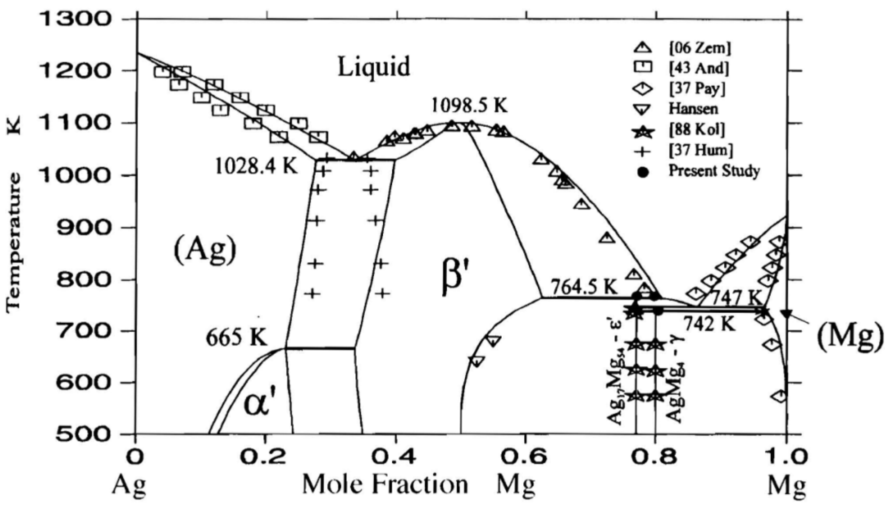

Figure 2-2: Calculated Ag-Mg phase diagram by Lim *et al.* [21]

Again, the enthalpies of mixing from Kawakami [20] were mistakenly reported in Lim's paper. Indeed, we noted that those values reported in Lim's paper are the same as those presented in Nayeb-Hashemi's paper. In addition, some phase diagram data were cited in different positions when compared with the original papers, and there was even some data that was not reported by the experimenters. For instance, the phase-boundary data between Ag phase and β' phase in Figure 2-2 were not mentioned by Hume-Rothery *et al.* [22]. Based on this observation, it is very likely that Lim did not check the data from the original paper and used them directly from the second-hand information that was mistakenly reported. Therefore, it is necessary to review all experimental data from the original papers.

2.2. Phase diagram data

Let us begin with phase diagram data. Żemcżużnyj [23] determined liquidus and solidus from 0 at% Mg to 100 at% Mg by thermal analysis. It is reported that the alloys were not stirred during the experiment, which can cause an incomplete reaction so that real information cannot be measured accurately. Moreover, four key invariant reactions were detected in this paper. One of them is the eutectic point ($\text{Liquid} \rightleftarrows \text{AgMg}_3\text{+HCP\_A3}$) that was reported as 742.15 K, but its real temperature may be a little higher based on the analysis above.

The solvus of the Mg phase (HCP) was investigated by Hume-Rothery *et al*. [22], and they confirmed that the eutectic temperature ($\text{Liquid} \rightleftarrows \text{AgMg}_3\text{+HCP\_A3}$) lies between 745.15 K and 748.15 K. Payne *et al*. [24] also detected this eutectic point at 745.15 K, which agrees well with Hume-Rothery's report. Moreover, the HCP_A3 rich phase diagram data were determined by thermal analysis. According to Payne's statement, the maximum uncertainty of temperature is 2 K.

The Ag-rich side (i.e., FCC phase) of the phase diagram was determined by Andrews *et al*. [25] by using both cooling and heating experiments, and their compositions were measured by microscopic examination. From the paper [25], it was noted that a slight amount of Mg was lost during the annealing process. Basically, the uncertainties for all data were provided by the authors.

Schürmann *et al*. [26] measured phase diagram data on the solvus of the Mg phase and the stoichiometric compound $AgMg_4$ by microprobe analysis. In fact, their data were not numerically reported but graphically presented. Hence the data from Schürmann *et al*. were digitized from the graph. Kolesnichenko *et al*. [27] investigated the Ag-Mg system on the HCP_A3 phase by using local X-ray probe analysis, differential thermal analysis and scanning electron microscopy. According to Kolesnichenko's report, the uncertainty of temperature is 2 K, and that of composition is 0.82 at% Mg.

2.3. Thermodynamic properties

Apart from phase diagram data, various thermodynamic properties have been made available in the following articles.

The heat capacity of the AgMg (B2_BCC) phase was calorimetrically determined by Schübel [28] with 50 at% Mg. The maximum uncertainty of the heat capacity is 1%. The mixing enthalpies of the liquid phase at 1323.15 K were determined by Kawakami [20] using drop calorimetry. Based on electrochemical method, the chemical potentials of Mg in the FCC phase and the B2_BCC phase were investigated between 623.15 K and 823.15 K by Kachi [29]. However, the author did not make a metallographic analysis to identify the phases. In this case, the results are dubious as the phase of the sample may not be exactly correct in his report, especially for those data that are close to the phase boundaries. In addition, the order-disorder change between the FCC and the $L1_2$ phase was also detected by Kachi [29]. According to the paper [29], an inflection point of electromotive force was observed by heating and cooling the sample. Furthermore, the variation in the specific heat of 23.3 at% Mg showed a typical shape of a λ transformation, which indicates that it could be a second-order transition. The second-order phase transformation was also confirmed by Fujiwara *et al*. [30] through calorimetric study: a typical λ type transformation was observed in the specific heat of 25.4 at% Mg. Buckley *et al*. [31] identified the range of ordering in the $L1_2$ phase by electrical resistance measurements. However, the data were not provided as numerical values, but graphically displayed. Moreover, again the authors did not give any analysis about the uncertainty of the data. In this case, we estimated the data as well as the uncertainty by digitizing the graph.

Trzebiatowski *et al.* [32] measured the chemical potential of Mg in the B2_BCC phase using the EMF method. According to the description, some samples were measured in Mg-rich side, which possibly belong to a two-phase region ($B2\_BCC{+}AgMg_3$) according to the latest phase diagram (Lim *et al*. [21]). Robinson *et al*. [33] determined the heat of formation of the compound B2_BCC by tin-solution calorimetry at 273.15 K, and they provided the precision of their measurements. Gangulee *et al*. [34] compared the heat of formation in a tin solution calorimeter on two parallel sets of specimens: one was quenched and the other was slowly cooled from 773 K to 273 K. Although a very small difference was observed, the slowly cooled alloys showed more short-range order than the quenched one did. The strong bond energy of the compound B2_BCC at temperatures below 273 K was confirmed by Jena *et al*. [35] as they obtained negative heat of formation that was calibrated by additions of tin.

The activities of Mg in the liquid phase were determined by Gran *et al*. [12] using the vapor pressure method. During the experiment, only temperature and composition of Mg were experimentally determined, and other properties can be calculated based on the experimental information. In [12], the uncertainties about the temperature and the composition were proposed.

2.4. Order-disorder transformation between the FCC and the $L1_2$ phase

As introduced above, the order-disorder transition between the FCC and the $L1_2$ phase was suggested as a second-order transition according to the thermodynamic data [29-31]. However, this statement contradicts that in Hämäläinen *et al*. [36]. In their report [36], a discontinuity of the thermal expansion coefficient between the FCC and the $L1_2$ phase was detected, which may be associated with a first-order transition. Furthermore, their statement was supported by the crystallographic data [37-39] as they also suggested a first-order transition. In fact, it is not easy to judge which paper should be more trustworthy because they all have evidence to support their reports. Therefore, the first-order and second-order transitions will be taken into account separately during the present assessment.

2.5. Data analysis

It is crucial to assign statistical uncertainties to experimental observations and conditions. However, most analysts prefer to carry out uncertainties based on their experience and knowledge to the experiments rather than statistical calculation. In fact, for most measurements in practice, we have no choice but to estimate uncertainties non-statistically because they just cannot be statistically calculated. To understand this point, it would be helpful to know how available methods for statistical calculation of uncertainty work.

Assume that the data are normally distributed. Then a general way to evaluate statistical uncertainties is as follows. We use

$$\bar{x}_{mean} = \frac{\sum_{i=1}^{n} x_i}{n} \tag{2.1}$$

to determine the mean from n repeated data at the same conditions, and then we calculate the statistical uncertainty ε (also called the standard deviation of measured values) by

$$\varepsilon=\sqrt{\frac{\sum_{i=1}^{n}\left(x_i-\overline{x}_{mean}\right)^2}{n-1}}. \tag{2.2}$$

It is meaningless to calculate such properties with a single or very few data. However, for most measurements in practice, repeated data are extraordinarily difficult to obtain because of two reasons. On one hand, some experimenters do not pay attention to the significance of replicating experiments. On the other hand, it is technically problematic to reproduce measurements under the same conditions, especially for some thermodynamic experiments.

Even though we have found a great deal of data from the literature, none of it is satisfactory for determining statistical uncertainties. Nevertheless, it is still significant to consider the uncertainties in a proper way. It is essential to pay attention to the uncertainty analysis from the literature whenever the uncertainties are mentioned. However, for those papers without uncertainty analysis, we have to estimate uncertainties by careful analysis of their measurement practices.

It should be emphasized that uncertainties in experimental conditions should also be taken into account. The method to calculate their statistical uncertainties is the same as previously discussed, but they also cannot be statistically calculated due to insufficient data. Consequently, the estimation of uncertainties in experimental conditions is also based on the information from the paper and analysts' experience.

When uncertainties in both experimental observations and conditions (or variables) are concerned, based on an assumption that uncertainties in different variables are independent and uncorrelated, one can calculate the overall uncertainty σ through the propagation of uncertainty formalism:

$$\sigma = \left(\left(\Delta y^{\text{observation}} \right)^2 + \sum_{i=1}^{n} \left(\left(\partial y^{\text{observation}} / \partial x_i \right) \cdot \Delta x_i \right)^2 \right)^{1/2}, \tag{2.3}$$

where $y^{\text{observation}}$ is the function of independent variables x_i, and n is the number of variables. $\Delta y^{\text{observation}}$ and Δx_i are uncertainties of experimental observation and conditions respectively. It is worth recalling the statistical weight w of Eq. (1.3), which is related to the overall uncertainty σ:

$$w = \sigma^{-2} \tag{2.4}$$

The uncertainties analyzed above only consider random error, which is a statistical fluctuation in the measured data due to the unpredictable variations of influential quantities. The value of the random error can be reduced by increasing the number of observations but cannot be removed. The other type of error is called systematic error, which is independent of numbers of observations and cannot be analyzed statistically. Nevertheless, the systematic error can be corrected by setting a specific weight to the data.

The purpose of weighting is to change the contributions for a set of equilibria: the default value of a weight is 1, which means nothing has changed; when it is greater than 1, such equilibria as an invariant reaction is treated as more important; and for some data that we do not trust as much, their weight would be assigned to be less than 1.

The details about each data that we accepted as well as their uncertainties and statistical weights are given in **Appendix I**.

3. Modeling

There are four substitutional solutions (liquid, B2_BCC and HCP_A3) and two intermediate phases ($AgMg_3$ and $AgMg_4$) in the Ag-Mg system. The importance of choosing a suitable Gibbs energy model is well-known. In general, a good Gibbs energy model should satisfy the following four criteria:

- Physical soundness
- Applicable in a reasonable temperature/pressure range
- Useful for multi-component systems
- Simplicity

3.1. Modeling in liquid and HCP_A3 phases

The liquid and HCP_A3 phases are treated by a substitutional-regular-solution model that is based on the assumption that atoms are randomly distributed in the solutions. The molar Gibbs energy is expressed as:

$$G_{\mathrm{m}}^{\theta} = \underbrace{x_{\mathrm{Ag}}^{\theta}\,{}^{0}G_{\mathrm{Ag}}^{\theta} + x_{\mathrm{Mg}}^{\theta}\,{}^{0}G_{\mathrm{Mg}}^{\theta}}_{{}^{\mathrm{srf}}G_{\mathrm{m}}^{\theta}} + \underbrace{RT(x_{\mathrm{Ag}}^{\theta}\ln x_{\mathrm{Ag}}^{\theta} + x_{\mathrm{Mg}}^{\theta}\ln x_{\mathrm{Mg}}^{\theta})}_{{}^{\mathrm{id}}G_{\mathrm{m}}^{\theta}} + {}^{\mathrm{ex}}G_{\mathrm{m}}^{\theta}. \tag{3.1}$$

The symbol θ can be either liquid or HCP_A3 phase. ${}^{0}G_{\mathrm{Ag}}^{\theta}$ and ${}^{0}G_{\mathrm{Mg}}^{\theta}$ are standard Gibbs energy of Ag and Mg in a phase respectively. The excess term ${}^{\mathrm{ex}}G_{\mathrm{m}}^{\theta}$ is used to describe the interactions between species, and it can be formulated by a Redlich-Kister series [40]:

$${}^{\mathrm{ex}}G_{\mathrm{m}}^{\theta} = x_{\mathrm{Ag}}x_{\mathrm{Mg}}\sum_{v=0}\left(x_{\mathrm{Ag}} - x_{\mathrm{Mg}}\right)^{v}\,{}^{v}L_{\mathrm{Ag,Mg}}^{\theta}, \tag{3.2}$$

where the parameter ${}^{v}L_{\mathrm{Ag,Mg}}^{\theta}$ can be temperature dependent:

$${}^{v}L_{\mathrm{Ag,Mg}}^{\theta} = {}^{v}a^{\theta} + {}^{v}b^{\theta}T + {}^{v}c^{\theta}T\ln T\cdots. \tag{3.3}$$

3.2. Modeling ordering in the L1$_2$ and the B2_BCC

The order-disorder transition occurs when temperature or composition changes. Usually the ordered state becomes disordered when the temperature increases. According to the information [29-32,34], the ordering state exists in the $L1_2$ and the B2_BCC phases. In order to simulate order-disorder transition, the model based on the compound energy formalism (CEF) is selected. The CEF was developed by Hillert and Staffansson [41] and was well described by Lukas *et al*. [42]. The structure of the phase can be implied by different sub-lattices. For the order-disorder transition, it requires at least two sub-lattices, and each sub-lattice is represented as a site of crystallographic structure. Figure 3-1 and Figure 3-2 show two possible ordering structures of the $L1_2$ phase, and they both can be described by a two sub-lattice model, but with different number of sites.

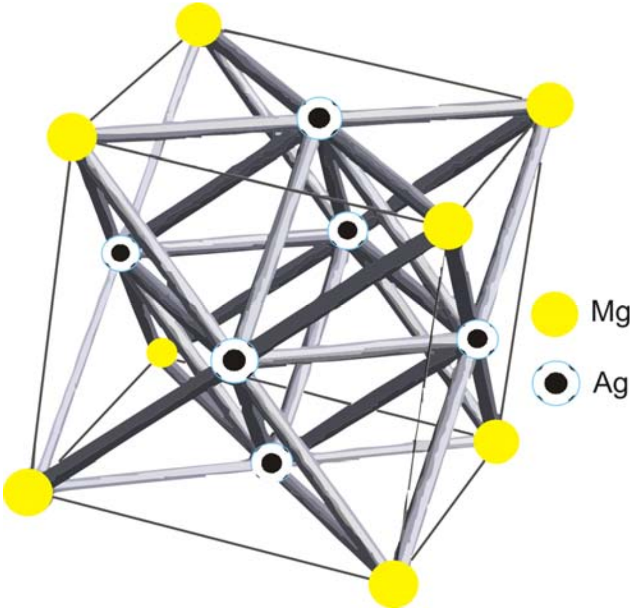

Figure 3-1: A complete ordering structure of the $L1_2$ phase.

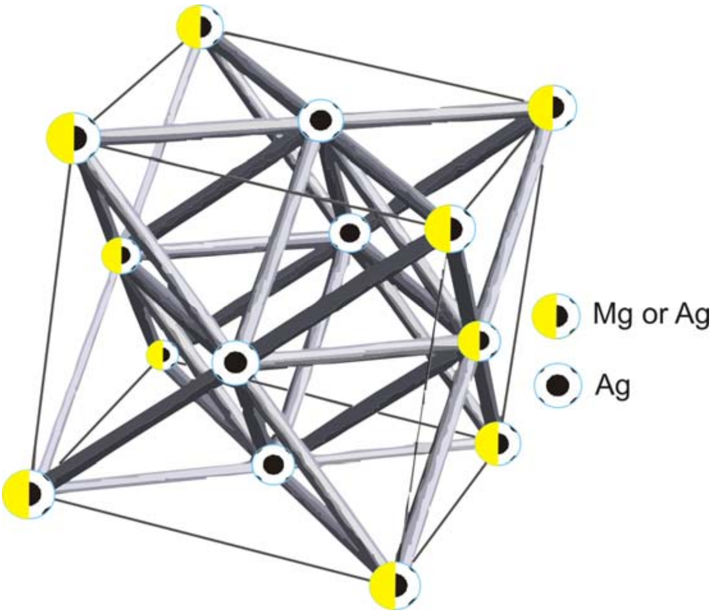

Figure 3-2: A partial ordering structure of the L1$_2$ phase.

Figure 3-1 displays two different sub-lattices: one is completely occupied by Mg atoms; the other one is entirely occupied by Ag atoms. This structure can be modeled with two sub-lattices after the formula $\left(\mathrm{Ag}_{y^1_{\mathrm{Ag}}},\mathrm{Mg}_{y^1_{\mathrm{Mg}}}\right)_{0.25}\left(\mathrm{Ag}_{y^2_{\mathrm{Ag}}},\mathrm{Mg}_{y^2_{\mathrm{Mg}}}\right)_{0.75}$, where y_i^j $\left(i=\mathrm{Ag},\mathrm{Mg};\, j=1,2\right)$ is the site fraction of i in the j sub-lattice. According to the structural information, the major component of the first sub-lattice should be Mg (i.e., $y^1_{\mathrm{Mg}}\approx 1$) as its number of sites is 0.25, and the major component of the second sub-lattice is Ag (i.e., $y^2_{\mathrm{Ag}}\approx 1$) because its number of sites is 0.75. Nevertheless, if the structure is not complete ordered, then it would present the case shown in Figure 3-2, which can be modeled as: $\left(\mathrm{Ag}_{y^1_{\mathrm{Ag}}},\mathrm{Mg}_{y^1_{\mathrm{Mg}}}\right)_{0.5}\left(\mathrm{Ag}_{y^2_{\mathrm{Ag}}},\mathrm{Mg}_{y^2_{\mathrm{Mg}}}\right)_{0.5}$: the first sub-lattice is randomly occupied by both atoms; in the second sub-lattice, the center of four faces are occupied by a majority of Ag atoms.

It should be emphasized that these two structures (Figure 3-1 and Figure 3-2) cannot be modeled with the same two sub-lattice model simultaneously, but they can be modeled with a four sub-lattice model: $\left(\mathrm{Ag}_{y^1_{\mathrm{Ag}}},\mathrm{Mg}_{y^1_{\mathrm{Mg}}}\right)_{0.25}\left(\mathrm{Ag}_{y^2_{\mathrm{Ag}}},\mathrm{Mg}_{y^2_{\mathrm{Mg}}}\right)_{0.25}\left(\mathrm{Ag}_{y^3_{\mathrm{Ag}}},\mathrm{Mg}_{y^3_{\mathrm{Mg}}}\right)_{0.25}\left(\mathrm{Ag}_{y^4_{\mathrm{Ag}}},\mathrm{Mg}_{y^4_{\mathrm{Mg}}}\right)_{0.25}$. For this four sub-lattice model, if the first sub-lattice is mainly occupied by Mg, while the other three sub-lattices are mainly occupied by Ag, then this case corresponds to the structure in Figure 3-1. If the first two sub-lattices are randomly mixed by Mg and Ag atoms, and the other two sub-lattices are mainly occupied by Ag, then this four sub-lattice model is used to model the second structure (Figure 3-2).

Figure 3-3 displays the ideal ordering unit cell in B2_BCC phase: it is preferable that the corners be occupied by atoms Mg, and atoms Ag are located at the center of the cell. This phase is modeled with two sub-lattices: $\left(\mathrm{Ag}_{y^1_{\mathrm{Ag}}},\mathrm{Mg}_{y^1_{\mathrm{Mg}}}\right)_{0.5}\left(\mathrm{Ag}_{y^2_{\mathrm{Ag}}},\mathrm{Mg}_{y^2_{\mathrm{Mg}}}\right)_{0.5}$.

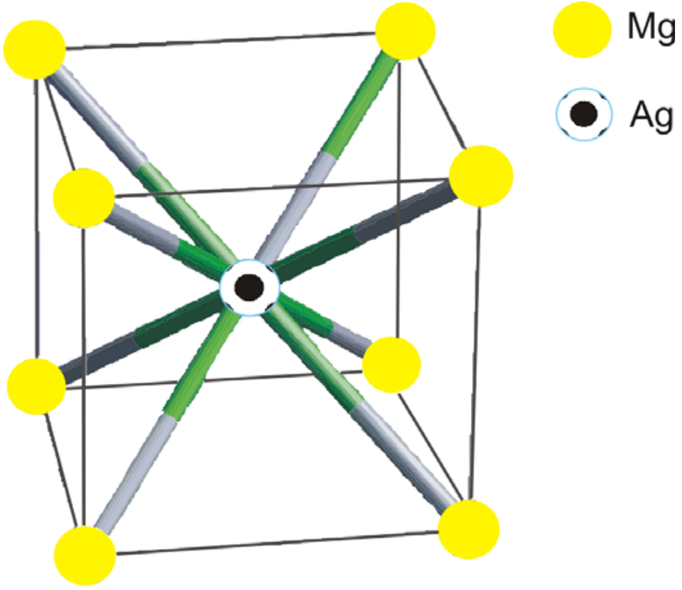

Figure 3-3: The ordering structure of B2_BCC phase.

To understand how the sub-lattice model is used, let us examine a case of a two sub-lattice model: $\left(\mathrm{Ag}_{y^1_{\mathrm{Ag}}},\mathrm{Mg}_{y^1_{\mathrm{Mg}}}\right)_i\left(\mathrm{Ag}_{y^2_{\mathrm{Ag}}},\mathrm{Mg}_{y^2_{\mathrm{Mg}}}\right)_j$.

Here i and j are the numbers of the sites of each sublattice, which satisfy:

$$i+j=1. \tag{3.4}$$

Accordingly, the overall composition of each component is related to their site fractions:

$$\begin{aligned} x_{\mathrm{Ag}} &= i\times y^1_{\mathrm{Ag}} + j\times y^2_{\mathrm{Ag}}, \\ x_{\mathrm{Mg}} &= i\times y^1_{\mathrm{Mg}} + j\times y^2_{\mathrm{Mg}}. \end{aligned} \tag{3.5}$$

[19]

The molar Gibbs energy with two sub-lattices is divided into the same three parts as Eq. (3.1) and they are:

$$\begin{aligned}
{}^{\mathrm{srf}}G_{\mathrm{m}}^{\theta} &= y_{\mathrm{Ag}}^{1} y_{\mathrm{Ag}}^{2}\,{}^{0}G_{\mathrm{Ag:Ag}} + y_{\mathrm{Ag}}^{1} y_{\mathrm{Mg}}^{2}\,{}^{0}G_{\mathrm{Ag:Mg}} + y_{\mathrm{Mg}}^{1} y_{\mathrm{Ag}}^{2}\,{}^{0}G_{\mathrm{Mg:Ag}} + y_{\mathrm{Mg}}^{1} y_{\mathrm{Mg}}^{2}\,{}^{0}G_{\mathrm{Mg:Mg}}, \\
{}^{\mathrm{id}}G_{\mathrm{m}}^{\theta} &= RT\left(i\times\left(y_{\mathrm{Ag}}^{1}\ln y_{\mathrm{Ag}}^{1} + y_{\mathrm{Mg}}^{1}\ln y_{\mathrm{Mg}}^{1}\right) + j\times\left(y_{\mathrm{Ag}}^{2}\ln y_{\mathrm{Ag}}^{2} + y_{\mathrm{Mg}}^{2}\ln y_{\mathrm{Mg}}^{2}\right)\right), \qquad (3.6) \\
{}^{\mathrm{ex}}G_{\mathrm{m}}^{\theta} &= y_{\mathrm{Ag}}^{1} y_{\mathrm{Mg}}^{1} \sum_{v=0}\left(y_{\mathrm{Ag}}^{1} - y_{\mathrm{Mg}}^{1}\right)^{v}\,{}^{v}L_{\mathrm{Ag,Mg:*}} + y_{\mathrm{Ag}}^{2} y_{\mathrm{Mg}}^{2} \sum_{v=0}\left(y_{\mathrm{Ag}}^{2} - y_{\mathrm{Mg}}^{2}\right)^{v}\,{}^{v}L_{\mathrm{*:Ag,Mg}}.
\end{aligned}$$

In order to describe the order-disorder transition, the total molar Gibbs energy ${}^{\mathrm{total}}G_{\mathrm{m}}^{\theta}$ is calculated by combining both disordered and ordered Gibbs energies:

$$ {}^{\mathrm{total}}G_{\mathrm{m}}^{\theta} = {}^{\mathrm{dis}}G_{\mathrm{m}}^{\theta}(x_{\mathrm{Mg}}) + {}^{\mathrm{ord}}G_{\mathrm{m}}^{\theta}. \qquad (3.7)$$

The term ${}^{\mathrm{ord}}G_{\mathrm{m}}^{\theta}$ represents the contribution due to ordering of the disordered state, and its value equals zero when it is disordered, i.e., $x_{\mathrm{Mg}} = y_{\mathrm{Mg}}^{1} = y_{\mathrm{Mg}}^{2}$. Thus, this term can be described as:

$$ {}^{\mathrm{ord}}G_{\mathrm{m}}^{\theta} = {}^{\mathrm{ord}}G_{\mathrm{m}}^{\theta}(y_{\mathrm{Mg}}^{1}) - {}^{\mathrm{ord}}G_{\mathrm{m}}^{\theta}(x_{\mathrm{Mg}} = y_{\mathrm{Mg}}^{1} = y_{\mathrm{Mg}}^{2}) \qquad (3.8)$$

Moreover, when the disorder is a stable state, ${}^{\mathrm{total}}G_{\mathrm{m}}^{\theta}$ will have an extremum.

The technique to model a four sub-lattice model is very similar to that of a two sub-lattice model, and they are mathematically equivalent. More details on this discussion can be found in [43].

3.3. Modeling in $AgMg_3$ and $AgMg_4$ phases

The two intermediate phases have been modeled in the same way as Lim *et al*. [21] did. $AgMg_3$ and $AgMg_4$ are treated as stoichiometric compounds that have no solubility ranges. They are both described with two sub-lattices: one sub-lattice is occupied by Ag only and the other is occupied by Mg only.

4. Optimization

4.1. Non-linear least squares method as a mathematical foundation of the CALPHAD technique

The optimization is based on using the least squares method that was implemented in the built-in module PARROT [44] of Thermo-Calc software [45]. In principle, this method can be classified as linearity and non-linearity in terms of the relationship between the parameters and the model: if the model is linear with respect to the parameters, then it is linear least squares; otherwise, it is non-linear least squares. Nevertheless, when the statistical weight is considered, then even if the model is linear to parameters, it may be still result in non-linearity. A simple illustration of the working of the CALPHAD technique was given by Eq. (1.3), and let us examine it again to discuss the reasons for non-linearity in the following subsections.

4.1.1. Causes of non-linearity

Uncertainties from independent variables: Δx_i

Independent variables are usually experimental conditions, such as temperatures and compositions when measuring the mixing enthalpy in experiment 1 of Eq. (1.3). According to Eq. (2.4), the statistical weight is given by Eq. (4.1):

$$w_i^{{}^{\mathrm{L}}H} = \frac{1}{\left({}^{\mathrm{L}}H_i^{\exp}\right)^2 + \left(\frac{\partial\, {}^{\mathrm{L}}H^{\mathrm{calc}}\left(x_{2_i}, T_i, {}^{\mathrm{L}}\vec{\mathrm{C}}\right)}{\partial x_2} \times \Delta x_{2_i}\right)^2 + \left(\frac{\partial\, {}^{\mathrm{L}}H^{\mathrm{calc}}\left(x_{2_i}, T_i, {}^{\mathrm{L}}\vec{\mathrm{C}}\right)}{\partial T} \times \Delta T_i\right)^2}, \qquad (4.1)$$

It is clear that Eq. (4.1) is non-linear to parameters ${}^{\mathrm{L}}\vec{\mathrm{C}}$, and it will result in non-linear least squares after substituting this equation into Eq. (1.3).

Phase diagram data between different phases

Let us recall experiment 3 in Eq. (1.3) where the liquidus were measured. In the equation, T^{calc} is derived from the common tangent law, while the chemical potential of each component in different phases sharing the same tangent is the same. To be more specific, it can be illustrated by the following equations that correspond to the case shown in Figure 4-1.

$$\mu_1^{\beta}(x_2^{\beta}, T, {}^{\beta}\vec{\mathrm{C}}) = \mu_1^{\mathrm{L}}(x_2^{\mathrm{L}}, T, {}^{\mathrm{L}}\vec{\mathrm{C}}), \tag{4.2}$$

$$\mu_2^{\beta}(x_2^{\beta}, T, {}^{\beta}\vec{\mathrm{C}}) = \mu_2^{\mathrm{L}}(x_2^{\mathrm{L}}, T, {}^{\mathrm{L}}\vec{\mathrm{C}}). \tag{4.3}$$

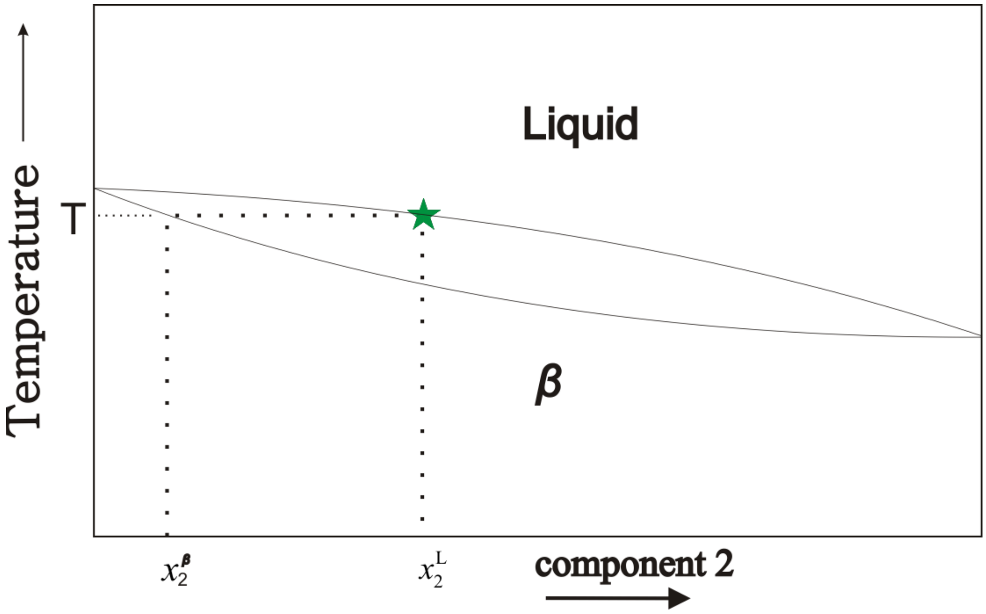

Figure 4-1: A postulated binary phase diagram.

Actually, in addition to the measured temperature, only x_2^{L} is a known experimental condition, while x_2^{β} is a hypothetical composition of the solidus at T. The reason for introducing such a hypothetical variable is to fulfill the common tangent law. Suppose that parameters ${}^{\beta}\vec{\mathrm{C}}$ and ${}^{\mathrm{L}}\vec{\mathrm{C}}$ are already known, then there are only two unknown variables (i.e., x_2^{β} and T) in Eqs. (4.2) and (4.3). Thus, it is capable to calculate these unknown variables by solving these two equations. It is worth noting that x_2^{β} appears in the entropy part, i.e., $RT\ln(1-x_2^{\beta})$ and $RT\ln x_2^{\beta}$. As a result, x_2^{β} and T both may be non-linear with respect to parameters ${}^{\beta}\vec{\mathrm{C}}$ and ${}^{\mathrm{L}}\vec{\mathrm{C}}$, and the deduction is given in Appendix II.

Thermodynamic properties of heterogeneous mixtures

Apart from the two cases above, there is another case for non-linear least squares. Again, for illustrative purposes, an example of how to calculate heat of formation in heterogeneous mixtures is presented below. Figure 4-2 displays the position where the heat formation was measured. Only composition $x_2^{\beta+\mathrm{L}}$ and temperature T are known experimental quantities.

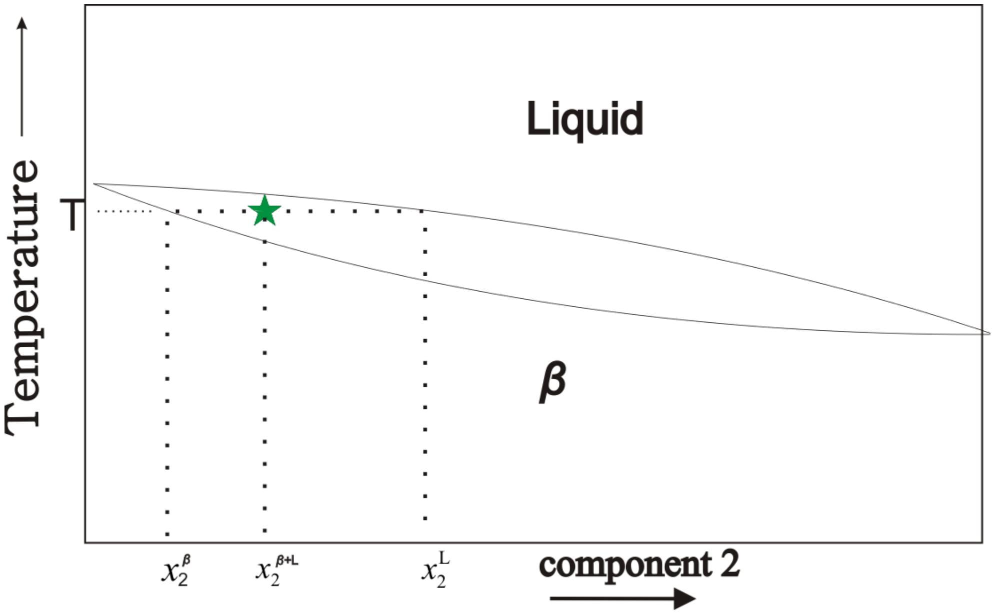

Figure 4-2: Heat formation measured in a two-phase (β+L) region.

In order to calculate the heat of formation in the two-phase region, we need to combine the information from both phases. In principle, the overall Gibbs energy $G^{\beta+\mathrm{L}}$ in a two-phase region is calculated by using the lever rule conditions, which gives:

$$G^{\beta+\mathrm{L}} = \frac{x_2^{\beta+\mathrm{L}} - x_2^{\beta}}{x_2^{\mathrm{L}} - x_2^{\beta}} G_{x_2^{\mathrm{L}}}^{\mathrm{L}} + \frac{x_2^{\mathrm{L}} - x_2^{\beta+\mathrm{L}}}{x_2^{\mathrm{L}} - x_2^{\beta}} G_{x_2^{\beta}}^{\beta}, \tag{4.4}$$

where $G_{x_2^{\mathrm{L}}}^{\mathrm{L}}$ and $G_{x_2^{\beta}}^{\beta}$ are defined as the Gibbs energy of liquid and β phases at the corresponding composition respectively, and $\frac{x_2^{\beta+\mathrm{L}} - x_2^{\beta}}{x_2^{\mathrm{L}} - x_2^{\beta}}$ as well as $\frac{x_2^{\mathrm{L}} - x_2^{\beta+\mathrm{L}}}{x_2^{\mathrm{L}} - x_2^{\beta}}$ are described as the amount of contribution from the liquid phase and β phase respectively. As mentioned before, x_2^{β} and x_2^{L} are unknown experimental conditions, but they can be calculated by solving Eqs. (4.2) and (4.3). Argued similarly as in the second case, x_2^{β} and x_2^{L} would be non-linear to the optimized parameters ${}^{\beta}\vec{\mathrm{C}}$ and ${}^{\mathrm{L}}\vec{\mathrm{C}}$. Thus, Eq. (4.4) is also non-linear to ${}^{\beta}\vec{\mathrm{C}}$ and ${}^{\mathrm{L}}\vec{\mathrm{C}}$ after substituting x_2^{β} and x_2^{L} into the equation. Moreover, it is obvious that the formalism of heat of formation is non-linear to ${}^{\beta}\vec{\mathrm{C}}$ and ${}^{\mathrm{L}}\vec{\mathrm{C}}$ as well.

4.1.2. Choosing an initial approach

Before optimizing parameters, it is necessary to determine their initial values. Of course, this work can be successful only if the model is correctly chosen. Good initial values make the convergence process faster, which means a minimum can be reached efficiently through the sum of squares. Poor initial values may need more time for convergence, or they may diverge, especially for non-linear least squares. However, it is not an easy job to find satisfactory initial values.

In general, there are two methods to determine initial values. One is based on the information from previous assessments; the other is based on the optimizers' experience and knowledge when they try to optimize a new system. Actually, this work can be very time-consuming if the initial values are not well-selected. In addition, this problem can be more serious to those inexperienced optimizers who usually determine initial values by guessing.

In the present study of assessing the Ag-Mg system, initial values of parameters were chosen based on the assessment of Lim *et al.* [21], where some additional constraints were used to avoid the calculation of unreasonable values.

4.2. Assessment procedure and results

The liquid phase was initially optimized, and the values of parameters were temporarily constrained by certain ranges when B2_BCC phase was considered. During the optimization of B2_BCC phase, the ordered state remained stable to its melting temperature, which verified the statement by Jordan *et al.* [46]. During the assessment to the FCC and the $L1_2$ phase, two possible types of order-disorder transition were considered: first and second order. We selected a four sub-lattice model $(\mathrm{Ag,Mg})_{0.25}(\mathrm{Ag,Mg})_{0.25}(\mathrm{Ag,Mg})_{0.25}(\mathrm{Ag,Mg})_{0.25}$ to describe this phase that contains a first-order phase transformation. In this case, the FCC phase was split into two phases that presented two composition sets. The composition set can be understood in this way: the number of phases that split from one phase is equal to the number of composition sets of this phase. Thus, one phase is always disordering, and the other is always ordering. When the transition becomes second order, some additional constraints should be added to sustain the optimization's best fit with available experimental data. A second-order transition means that the order parameter gradually decreased to zero by increasing the temperature, and thus only one composition set is required to simulate this transition. We chose a two sub-lattice model $\left(\mathrm{Ag,Mg}\right)_{0.5}\left(\mathrm{Ag,Mg}\right)_{0.5}$ instead of using $\left(\mathrm{Ag,Mg}\right)_{0.25}\left(\mathrm{Ag,Mg}\right)_{0.75}$ as the latter cannot reproduce the available data. It should be noted that the disordered phase and the ordered phase belong to the same phase. In order to distinguish these two states, we need to add some additional constraints on experimental data. As explained before, whether a phase is disordered or ordered can be identified by the site fraction, and this can be further understood by using a two sub-lattice model $\left(\mathrm{Ag}_{y_{\mathrm{Ag}}^{1}},\mathrm{Mg}_{y_{\mathrm{Mg}}^{1}}\right)_{i}\left(\mathrm{Ag}_{y_{\mathrm{Ag}}^{2}},\mathrm{Mg}_{y_{\mathrm{Mg}}^{2}}\right)_{j}$, where the order parameter s is defined as:

$$s=\left(y_{\mathrm{Mg}}^{2}-y_{\mathrm{Mg}}^{1}\right)^{2}. \tag{4.5}$$

A state is disordered when $s=0$, and a state is completely ordered when $s=1$, and a state is partially ordered when $0<s<1$. Thus, the information of the order parameter was included to distinguish between disordered and ordered states.

In addition to the phases discussed above, the thermodynamic description of HCP_A3, $\mathrm{AgMg_3}$ and $\mathrm{AgMg_4}$ phases are the same as Lim *et al.* [21] reported. An updated table of parameters for all phases is listed in Appendix III. The calculated phase diagrams of the two cases discussed above are shown in Figure 4-3 and Figure 4-4. In addition, the invariant temperatures are listed in Table 4-1.

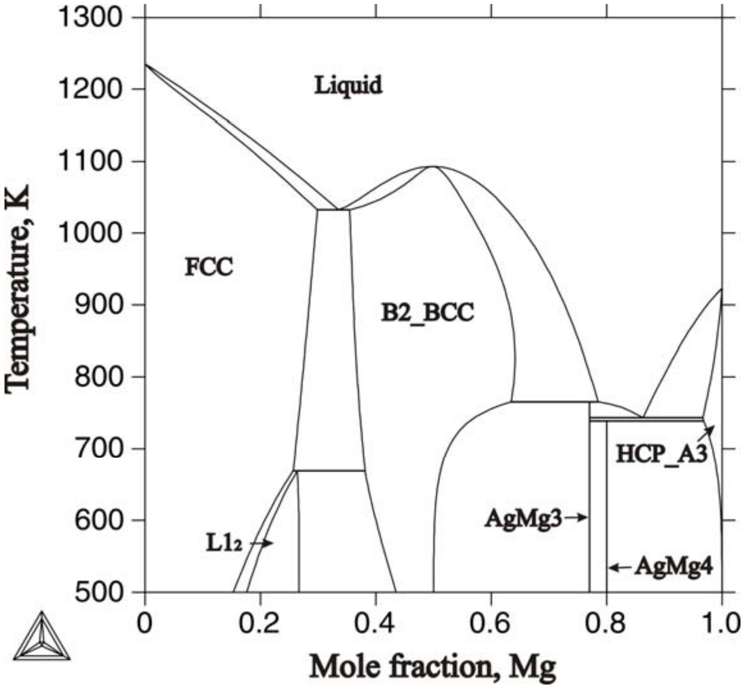

Figure 4-3: The calculated Ag-Mg phase diagram from the present assessment, where the order-disorder transition is first-order.

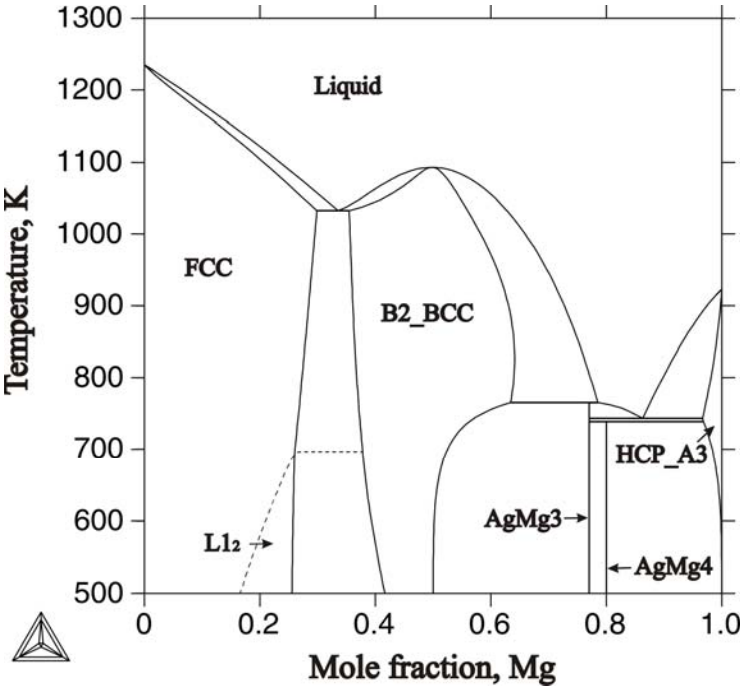

Figure 4-4: The calculated Ag-Mg phase diagram from the present assessment, where the order-disorder transition is second-order (dashed line).

Table 4-1: The invariants of the Ag-Mg system.

Invariant equilibrium	T(K) [19]	T(K) [21]	T(K) (This work)
Liquid $\rightleftarrows$ FCC+B2_BCC	1032.45	1033	1032.37
Liquid $\rightleftarrows$ B2_BCC	1093.15	1093	1093.14
$AgMg_3$ $\rightleftarrows$ Liquid+B2_BCC	765.15	764	765.29
Liquid $\rightleftarrows$ HCP+$AgMg_3$	745.15	745	743.28
$AgMg_4$ $\rightleftarrows$ HCP+$AgMg_3$	–	742	738.61

4.2.1. Equilibria with the liquid

Figure 4-5 shows the calculated mixing enthalpy with experimental data that contain reasonable uncertainties. As we can see, the calculation crosses through most data.

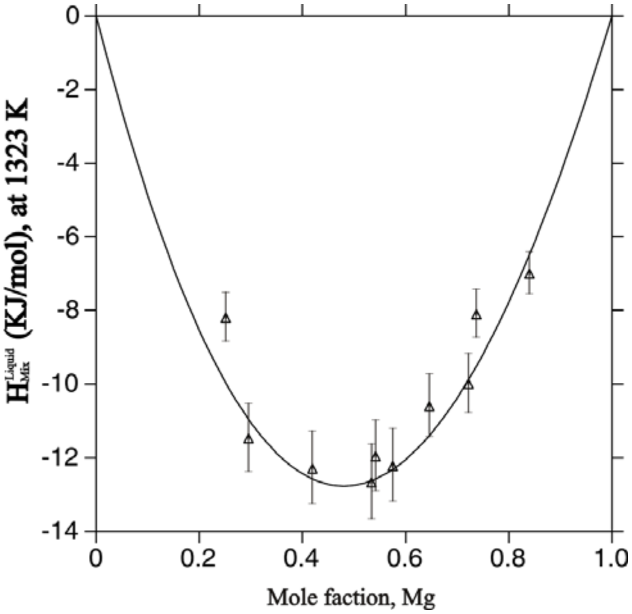

Figure 4-5: The calculated enthalpy of mixing at 1323 K, compared with experimental data [20].

In Figure 4-6 the activities of Mg were calculated at temperatures that are much higher than the melting point of all compositions. Although the measured data at different temperatures are close to each other, the activity of Mg is a little higher at lower temperatures.

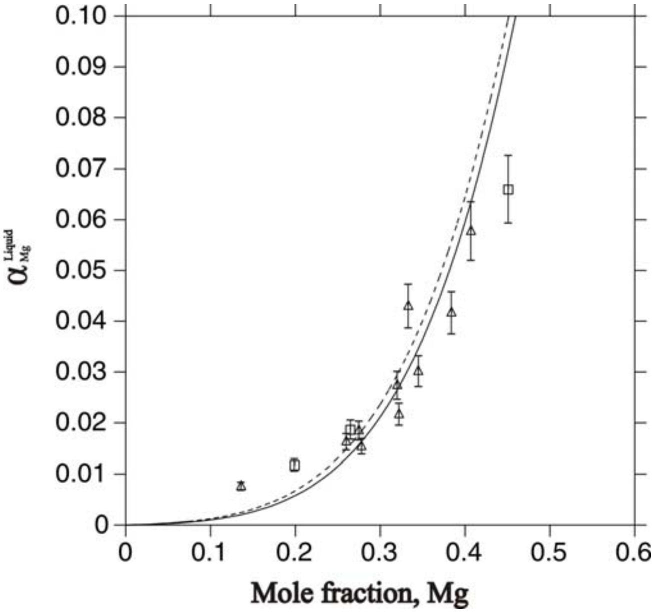

Figure 4-6: The calculated activity of Mg in the liquid. The dashed line was calculated at 1573 K that corresponds to □, the solid line was calculated at 1673 K that corresponds to △ [12].

Compared with the phase diagram data that was collected from many papers, the liquidus and solidus were well reproduced by these calculations (Figure 4-7).

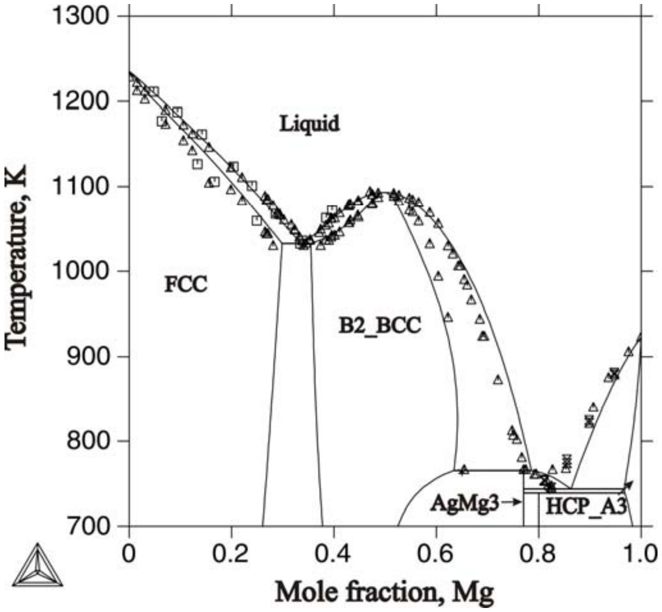

Figure 4-7: The calculated phase diagram for the liquid in equilibrium with FCC, B2_BCC, $AgMg_3$ and HCP_A3 compared with experimental data. The experimental data for the liquidus and solidus are from △ [23] □ [25] ◇ [22] ⧖ [24] ∗ [21].

4.2.2. Equilibria with B2_BCC phase

In Figure 4-8, the curve of the calculated heat capacity is a little higher than the measured data, but with acceptable ranges.

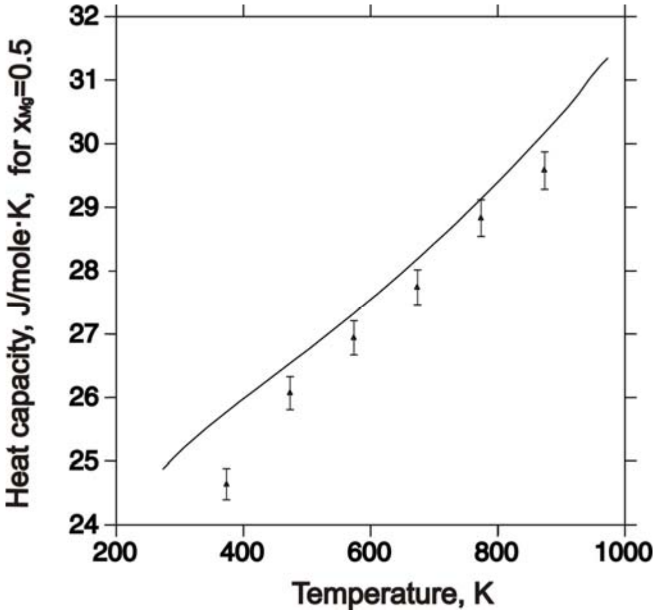

Figure 4-8: The calculated heat capacity in B2_BCC phase, compared with experimental data [28].

Figure 4-9 shows the chemical potentials of Mg calculated at several different compositions for the purpose of comparing with experimental data. Even though some calculated curves are not perfectly consistent with the experimental data, the overall tendency of data is properly simulated.

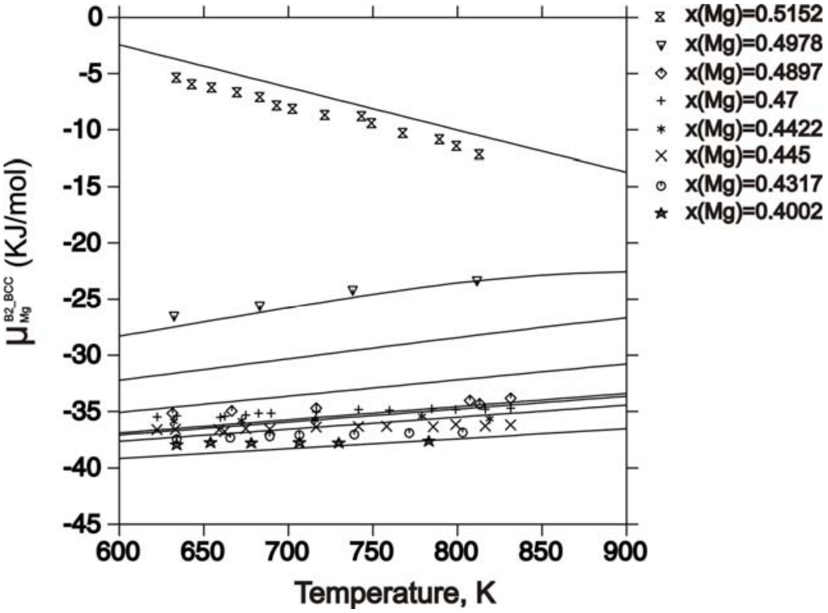

Figure 4-9: The calculated chemical potential of Mg in B2_BCC phase, compared with the experimental data [29].

The heat of formation in B2_BCC phase was calculated at 273.15 K, as displayed in Figure 4-10. Although it may not be a sound idea to use data at such a low temperature, the result shows a reasonable agreement.

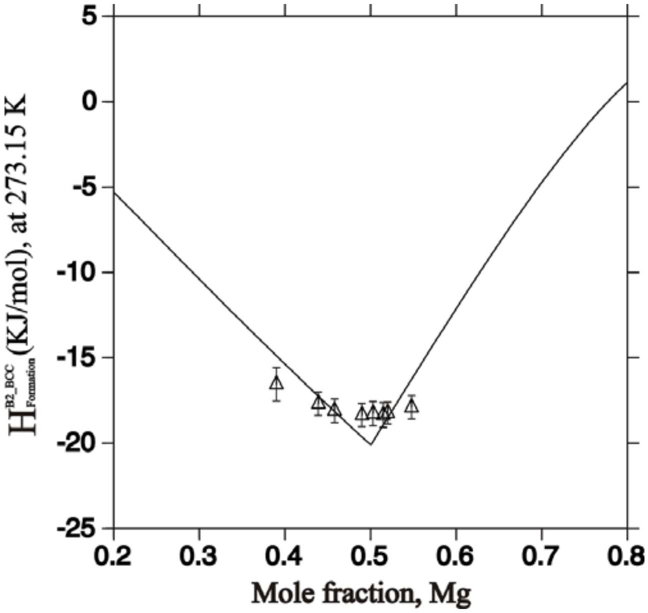

Figure 4-10: The calculated heat of formation in B2_BCC phase, compared with the experimental data [33].

4.2.3. Equilibria with the FCC and the $L1_2$ phase

The FCC and the $L1_2$ phase have an order-disorder transformation that could either be first-order or second-order. Figure 4-11 shows a magnification of the region where the transition is first-order. The fit to the phase diagram data is good, and a peritectoid transformation was calculated, i.e., $\mathrm{FCC+B2\_BCC} \rightleftarrows \mathrm{L1_2}$.

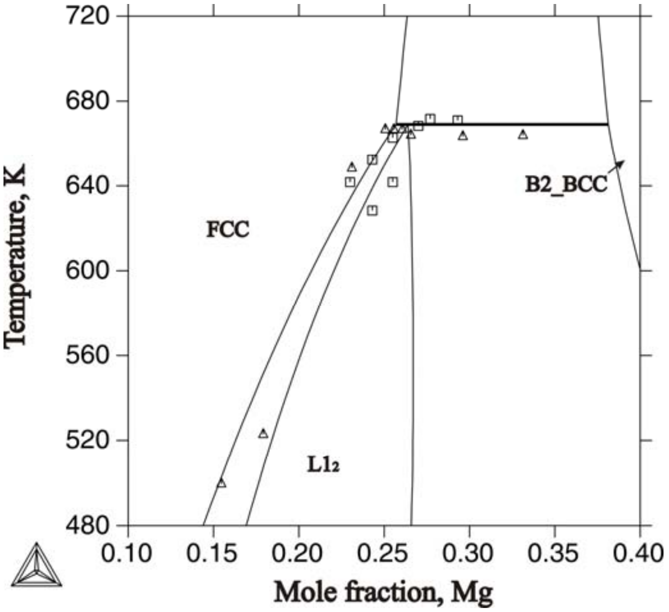

Figure 4-11: The calculated first-order transition line together with experimental data: △ [30], □ [31].

When the transition is treated as second-order, the order parameter *s* can be calculated by Eq. (4.5), as shown in Figure 4-12. As temperature increases from 300 K, *s* gradually decreases to zero, which means that the state becomes disordered.

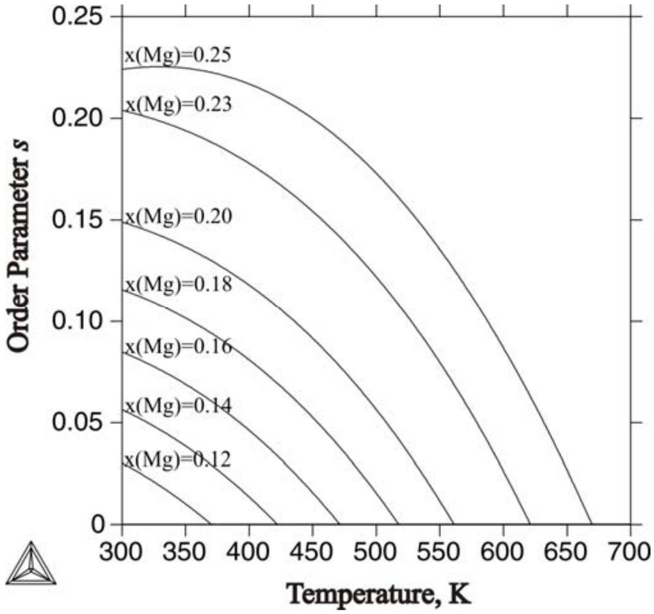

Figure 4-12: The calculated order parameter *s* for different compositions from 300 K to 700 K.

According to the information obtained from Figure 4-12, we are able to determine the second-order transition line between the FCC and the $L1_2$ phase, as shown in Figure 4-13.

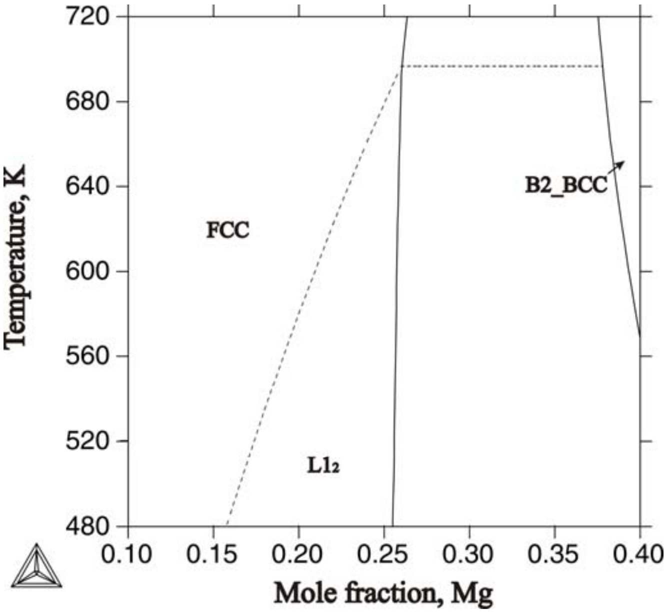

Figure 4-13: The calculated second-order transition line of the order-disorder transition between the FCC and the $L1_2$ phase.

In Figure 4-14, the calculated chemical potentials of Mg in the FCC phase for different compositions have reproduced the basic features, i.e., the values steadily decline as the temperature increases.

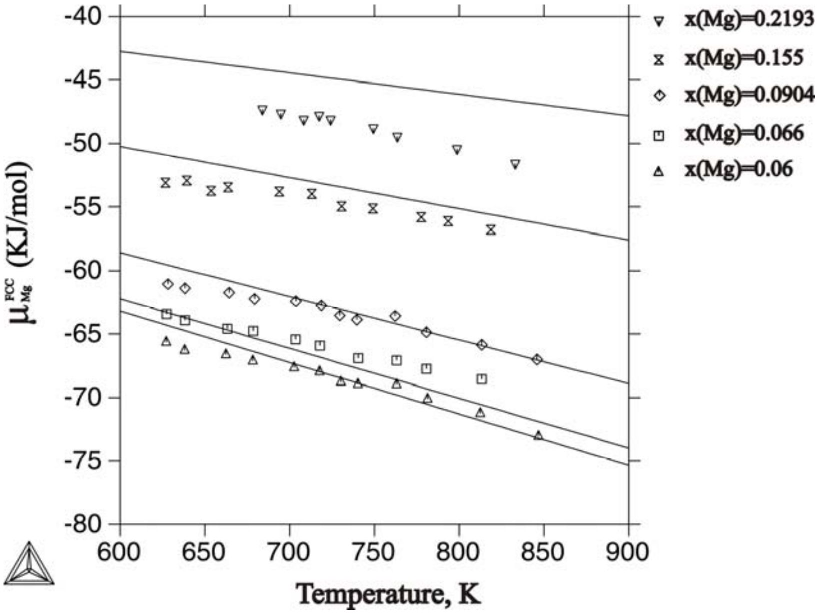

Figure 4-14: The calculated chemical potential of Mg in FCC phase, compared with the experimental data [29].

5. The conclusions of the assessment: can we do better?

All available data were carefully scrutinized and analyzed, and their uncertainties were reasonably estimated. This contribution should be helpful in future assessments that contain the Ag-Mg system. Furthermore, based on the thermodynamic description of the present assessment, most experimental data were satisfactorily reproduced. More importantly, we successfully described first- and second-order transformations by employing a four sub-lattice and a two sub-lattice model respectively.

The CALPHAD technique was employed during the present assessment. Undoubtedly, it demonstrated a powerful ability for thermodynamic optimization. In fact, almost all methods in a real world have their advantages and disadvantages; just as a coin has two sides, so does the CALPHAD technique. During the assessment, we have found three deficiencies that are usually ignored by others.

The first problem was already mentioned in the data analysis of Section 2.5: statistical uncertainties are minimally visible due to insufficient repeated data. However, uncertainties should always be taken into account during optimization. They are usually estimated by assigning error bars. In general, an error bar is represented by an experimental data with two bounds. If the data distribution follows a normal distribution, then the central point of the error bar is treated as the most probable data. Nevertheless, it is a serious mistake to use error bars if uncertainties cannot be statistically calculated. Without enough repeated data, there would be no way to determine the data distribution, and it is unreasonable to treat an experimental point as a central point of an error bar.

Another problem presented by the CALPHAD technique is how to choose a sound model, which was briefly mentioned at the beginning of Chapter 3. Even though we have some criteria for a good model, sometimes there is not enough information to help us to make the right decision. In other words, it might be not be problematic that a model can be replaced by another if they both can reproduce available data. However, it does not mean that both of them can be accepted. Thus, it is necessary that more criteria be considered.

The last problem is related to the algorithm of least squares. As explained in Subsection 4.1.2, initial values of parameters are always requisite and important, but they are usually determined under the condition of uncertainty. Moreover, it is difficult to judge whether the initial values are appropriate or not.

To solve the first problem, we recommend that the experimenters create many repeated experimental data, so that statistical uncertainties can be calculated. However, this solution may not be realistic, as it is too difficult to achieve in practice. For the other two problems, the availability of more information should help to decide the model and parameter values. Therefore, instead of improving the CALPHAD technique, an alternative idea is proposed to focus on solving these outstanding problems.

6. Non-statistical modeling

6.1. Kantorovich's idea

Non-statistical modeling is based on Kantorovich's idea [47]; instead of calculating statistical uncertainties, experimental data can be represented by reasonable finite intervals that describe all possible values of observation. Compared with the traditional error bar, each interval is constrained by an upper bound and a lower bound, as shown in Figure 6-1. An obvious difference is that there is not a central point between two bounds of the intervals. The reason for using intervals to describe data can be derived from the definition of the interval: it is a finite scale that contains all possible experimental observations at the same experimental conditions, so all points in this range are equally treated. In other words, the interval does not care about data distribution because all types of distribution are likely in it. Thus, the interval can be estimated without statistical calculation, and this overcomes the first problem where error bars are wrongly used.

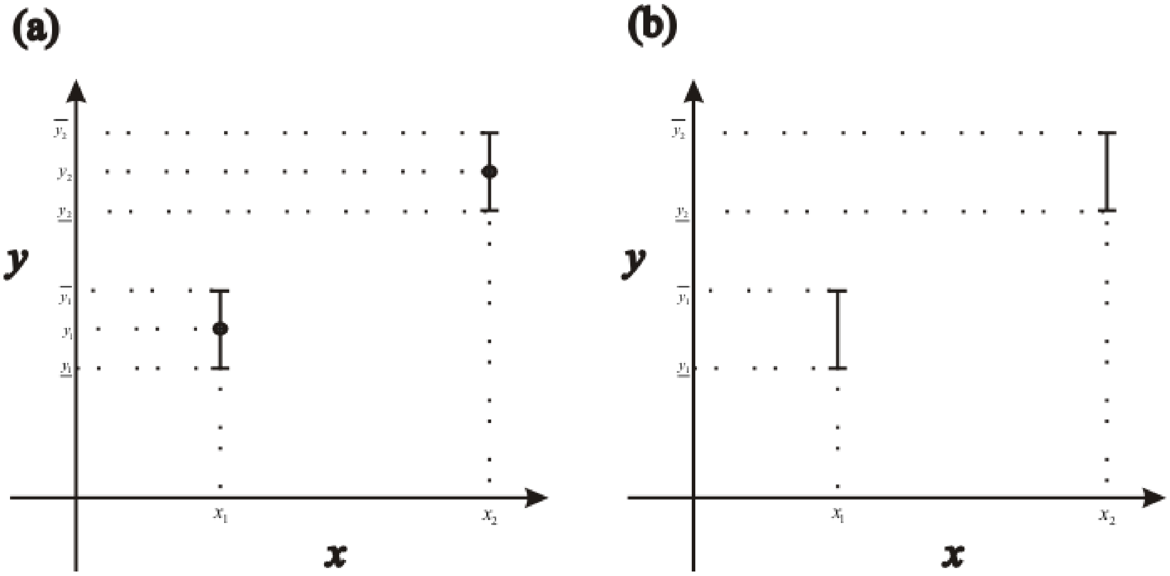

Figure 6-1: Error bars (a) and intervals (b).

6.2. Methodological aspects

Intervals cannot be applied to least squares because a unique experimental point does not exist. Thus, we need to find a method that is specific to the characteristics of the interval.

Before introducing the method, let us first identify what conditions should be satisfied in order to obtain satisfactory parameters. According to the definition of interval, possible experimental data should exist between the two bounds. Moreover, the data can be simulated by a model. Based on these two prerequisites, if the calculations of the model satisfy the constraints of all intervals, then the model's parameters should be accepted. From a mathematical viewpoint, this relationship can be described by inequalities. Let us examine a case of Figure 6-1 (b), which gives us the following:

$$\begin{aligned} \underline{y_1} \le f\left(x_1, \vec{\mathrm{C}}\right) \le \overline{y_1}, \\ \underline{y_2} \le f\left(x_2, \vec{\mathrm{C}}\right) \le \overline{y_2}. \end{aligned} \tag{6.1}$$

Here, $f\left(x\right)$ is a selected model and $\vec{\mathrm{C}}$ are parameters. If all inequalities are fulfilled, then $\vec{\mathrm{C}}$ are feasible parameters. When it is graphically represented, the calculations of the model must cross through all the intervals. Actually, it is possible that there might be more than one line that meets with this requirement, as shown in Figure 6-2. As each line is calculated from a model with a set of parameters, different lines imply different sets of parameters that may constitute a feasible region of parameters.

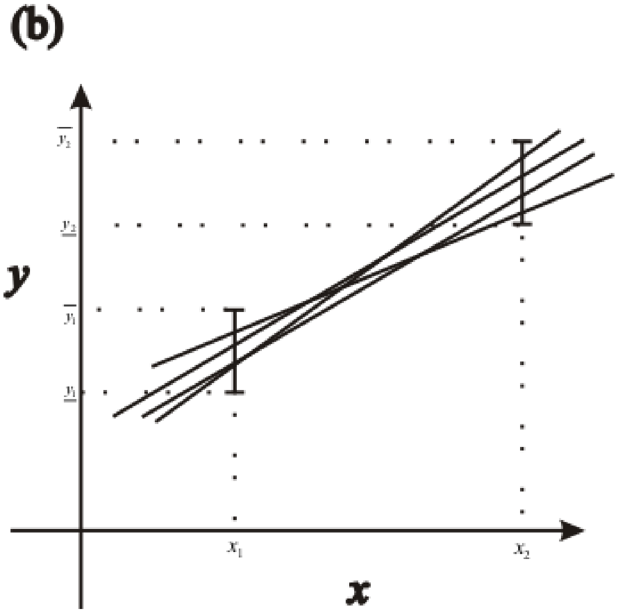

Figure 6-2: Different lines cross through intervals.

The next section will present the algorithm to solve those inequalities in order to obtain a feasible region of parameters. We offer a preliminary explanation of the following expressions:

- **A feasible region** consists of all feasible values of parameters if they exist; otherwise, it would be empty.
- The number of parameters of the model is called the **dimension of the feasible region**. For example, if there is only one parameter, then a feasible region is a line segment in one dimension where the axis is the parameter itself; if there are two

parameters, then a feasible region would be a polygon in two dimensions where each axis can be one of the parameters; if there are three parameters, then a feasible region would be a polytope in three dimensions.

- **A vertex** of a feasible region represents values of a set of parameters. Its corresponding calculation of the model should touch at least one bound of the intervals, but the calculation may not satisfy all the inequalities.
- **An extreme vertex** of a feasible region also represents values of a set of parameters, and its corresponding calculation of the model satisfies all the inequalities.
- **An outlier** is defined as a bad experimental value, and it would generate no feasible region.

6.3. Algorithmic and computational aspects

The calculation of feasible values of parameters is an NP-hard (Non-deterministic Polynomial-time hard) problem [48]. Although some methods were discussed by Walter *et al.* [49], it is very inconvenient to use them practically. In this section, we will propose an approach that is more efficient and effective to determine feasible values of parameters. A complete procedure of the method is described below:

Step 1 is to determine a reasonable interval for each observation by data analysis. This work requires all available information, such as knowledge of equipment, experimental procedures and analytical experience, to help with the estimation.

Step 2 is to choose a suitable model to simulate the data. As described before, the calculation of the model is supposed to be constrained by the two extreme bounds of each observation, and this relationship can be represented by inequalities.

Step 3 is to obtain values of vertices by calculating intersections of all inequalities. Suppose that there are n different linear inequalities, and each inequality contains m different unknown parameters (note that $\frac{n}{2} \geq m$). In order to calculate the m parameters, we need at least m equations. How do we obtain the equations? All inequalities are changed into equalities, which means that the inequality symbols are simply changed to equality symbols. Then we randomly select m different equalities from n equalities to constitute simultaneous equations and calculate a vertex that consists of m parameters. The number of vertices is determined by the number of combinations of equalities $C(n, m)$:

$$C(n,m) = \frac{n!}{(n-m)!m!}. \tag{6.2}$$

It should be mentioned that not all combinations can be accepted. The calculation of simultaneous equations cannot proceed if the solution is an empty set. For the convenience of the following description, we suppose that k vertices are obtained.

Step 4 is to find the extreme vertices. The reason for finding extreme vertices is that the values of some vertices may not satisfy all the inequalities. Thus, we need to substitute the values of k vertices back into the model to compare their calculations with all the inequalities to find those extreme vertices. If j $(j \geq 1)$ extreme vertices are obtained, then go to step 5; otherwise, we proceed to step 6 when there is no extreme vertex.

Step 5 is to construct a feasible region graphically when the number of parameters is no more than three. The reason will be discussed in Subsection 6.5.2.

Step 6 is to find outliers and reassign their intervals. A Simplex algorithm [50] is employed to find outliers by enlarging their intervals to approach the calculation. Thus, there will be only one set of feasible parameters in the final result. It is worth noting that a badly selected model may also lead to no feasible region. This statement will be discussed later.

This algorithm has been implemented in MATLAB script-language during the present study, and this program will be discussed in Appendix IV.

6.4. Practical implementations of non-statistical modeling

A simple illustration of implementing non-statistical modeling of imaginary experimental data is described in this section. Figure 6-3 shows a transition of the experimental data from the description of individual points to intervals.

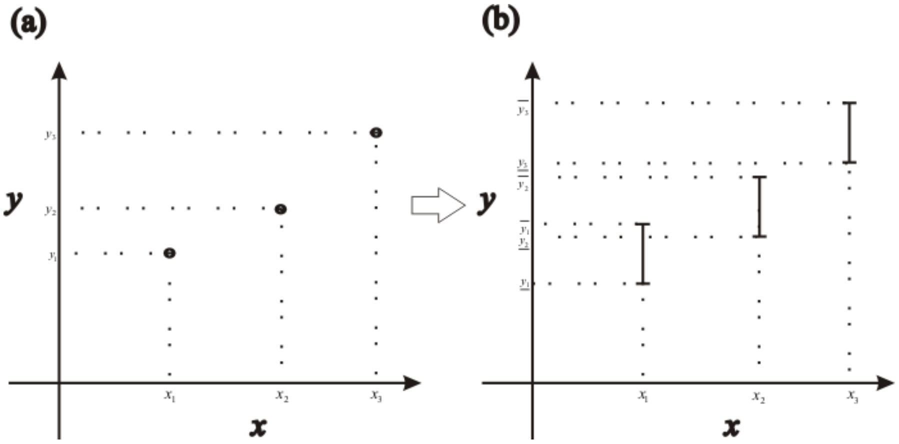

Figure 6-3: The original data (a) and the intervals (b).

Let us assume that a linear function $y = a + b \times x$ (a and b are parameters) is used to simulate the data. Then we will have three sets of inequalities:

$$\underline{y_i} \le a + b \times x_i \le \overline{y_i},\ (i = 1,2,3). \tag{6.3}$$

Changing inequality symbols to equality symbols gives six equations:

$$a + b \times x_i = \underline{y_i}, \tag{6.4}$$

$$a + b \times x_i = \overline{y_i}. \tag{6.5}$$

With two parameters and six equations, the number of combination is $C(6,2) = \frac{6!}{(6-2)!2!} = 15$. After calculating 15 sets of simultaneous equations, there are 12 vertices as shown in Figure 6-4. However, only six of them are extreme vertices that can constitute a feasible region.

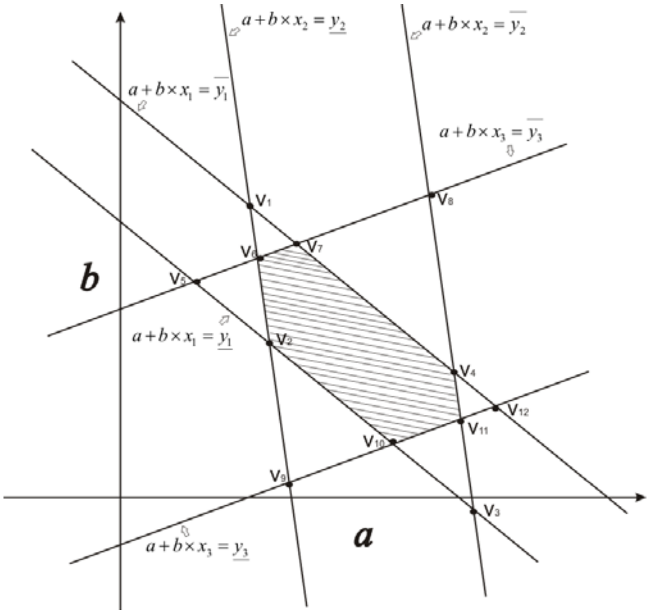

Figure 6-4: A feasible region of parameters *a* and *b*.

6.5. Methodological advantages and computational disadvantages of non-statistical modeling

Non-statistical modeling is able to avoid the problem of calculating statistical uncertainty, which makes use of insufficient experimental data possible. In addition, not only are no initial values of parameters required in this method, but it may also provide a feasible region of parameters. Furthermore, this method is helpful to determine a suitable model, as we know that a feasible region exists only if all inequalities are satisfied. Thus, the calculations of the model must meet with all inequalities. With this criterion, we may find a more satisfactory model.

However, recalling that almost all methods have their limitations, so does this method: its disadvantages are described in the following three cases.

6.5.1. Non-linear inequalities

A non-linear inequality means the selected model is non-linear to unknown parameters. So far, we have not found a method to overcome the problem of non-linear inequalities because it is a very difficult mathematical problem, but it is meaningful to discuss its complexity. The feasible region for linear inequalities is always a convex polytope that consists of flat planes, except in the case of a one-dimensional feasible region. By using the available program, the extreme vertices are convenient to find. However, it would be a disaster for non-linear inequalities. Some studies [51,52] have shown that a feasible region for non-linear inequalities would be an irregular and even discontinuous hypersurface, which means that separate feasible regions might exist. For illustrative purposes, Figure 6-5 gives two imaginary feasible regions that are created from two groups of data, and the overlaps are the intersections between the two regions.

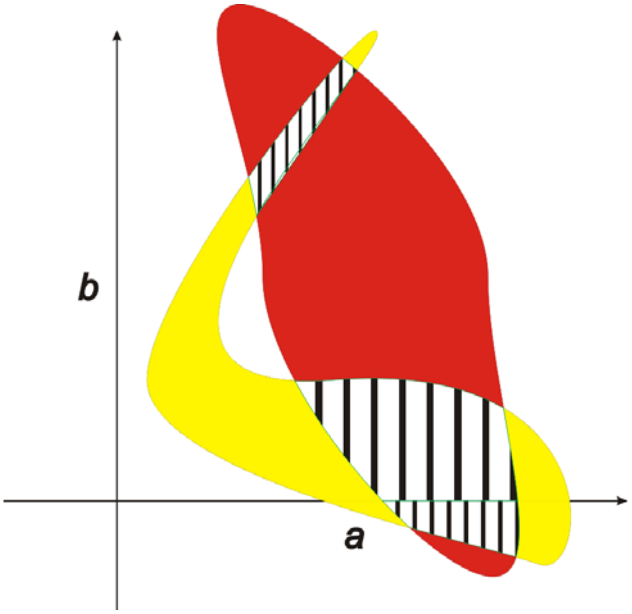

Figure 6-5: A hypothetical feasible region for non-linear inequalities and the overlaps are striped areas.

6.5.2. Multidimensional problems

The visualization of a feasible region requires the construction of extreme vertices by using different methods with regard to the particular dimension of a feasible region. In principle, it is easy to imagine a graph visualized in one-, two- and three-dimensions. However, it would be unnatural to visualize a picture in four- or even higher-dimensional spaces. Some attempts toward data visualization in high dimensions were discussed in [53,54].

6.5.3. Uncertainties in experimental conditions

In non-statistical data treatment, uncertainties in experimental conditions can also be treated as finite intervals. As a result, it is not hard to imagine that each data can be represented as a rectangle. Figure 6-6 is an example to show data described as a rectangle. Here, it is essential to define what the criterion of a good model is when the calculations of the model cross through a rectangle. In Figure 6-6, there are five lines, and all of them are calculated from an imaginary model. The differences among these lines are described below:

Line (1): $\exists\, x \in \left[\underline{x_1}, \overline{x_1}\right]$, we have $\underline{y_1} \le y \le \overline{y_1}$, which means it can cross through anypart of the rectangle, or even just touch a corner.

Line (2) (the dotted line): $\forall\, y \in \left[\underline{y_1}, \overline{y_1}\right]$, we have $\underline{x_1} \le x \le \overline{x_1}$, which means when $y \in \left[\underline{y_1}, \overline{y_1}\right]$, the inequality $\underline{x_1} \le x \le \overline{x_1}$ must be always satisfied.

Line (3) (the long-dash line): $\forall\, x \in \left[\underline{x_1}, \overline{x_1}\right]$, we have $\underline{y_1} \le y \le \overline{y_1}$, which means the inequality $\underline{y_1} \le y \le \overline{y_1}$ must be always satisfied when $x \in \left[\underline{x_1}, \overline{x_1}\right]$.

Lines (4) and (5):

$\forall\, x \in \left[\underline{x_1}, \overline{x_1}\right]$, we have $\underline{y_1} \le y \le \overline{y_1}$, and $\forall\, y \in \left[\underline{y_1}, \overline{y_1}\right]$, we have $\underline{x_1} \le x \le \overline{x_1}$.

Which line should be chosen as a good calculation? The answer is that all of them are satisfactory to obtain feasible values of parameters. According to the definition of the interval and rectangle data, any values in the region are possible data that should be equally treated. Therefore, feasible values of parameters can be obtained if the model crosses through any part of the rectangle.

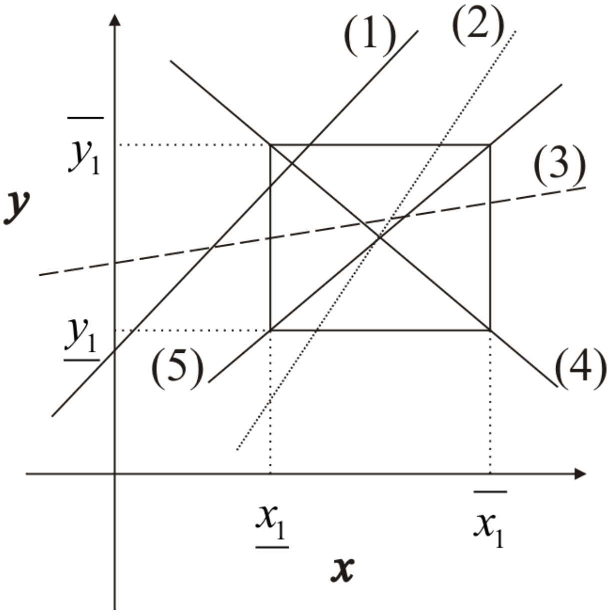

Figure 6-6: Experimental data in a description of a rectangle, with five calculated lines.

As the description of experimental data has changed, the feasible region should be constructed in a different way. The first step is to generate a feasible region from one rectangle that is the union of all feasible parameters; then the final feasible region is the intersection of all feasible regions previously obtained. In order to have a better understanding, Figure 6-7 is an example of two experimental data that are described by non-statistical treatment (*x* axis is defined as an experimental condition and *y* axis is defined as an experimental observation).

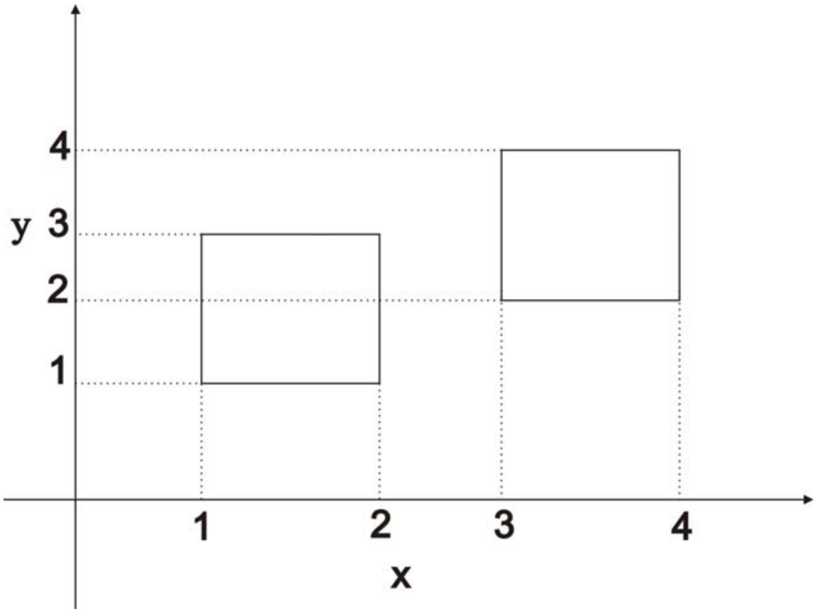

Figure 6-7: An assumed example with uncertainties in both experimental conditions and observations.

For simplification, a linear model is used to simulate the data:

$$y = a + b \times x, \tag{6.6}$$

where a and b are two unknown parameters. According to the criterion defined above, feasible values of a and b can be obtained if they satisfy the following inequalities:

$$\exists\, x \in [1,2], \text{ we have } 1 \le a + b \times x \le 3, \text{ and } \exists\, x \in [3,4], \text{ we have } 2 \le a + b \times x \le 4. \tag{6.7}$$

Solving Eq. (6.7) requires infinite calculations because the inequalities will be checked for every single point of the range of x. This algorithm cannot be implemented by a program, due to the limitation of the computational technique. Fortunately, the present example is unique because the feasible region can be obtained by just solving 4 inequalities. At first, the feasible region for each rectangle is the union of all feasible parameters, and then the final feasible region is the intersection of the previous two feasible regions. Figure 6-8 shows the final feasible region that is not a convex polygon but a concave polygon.

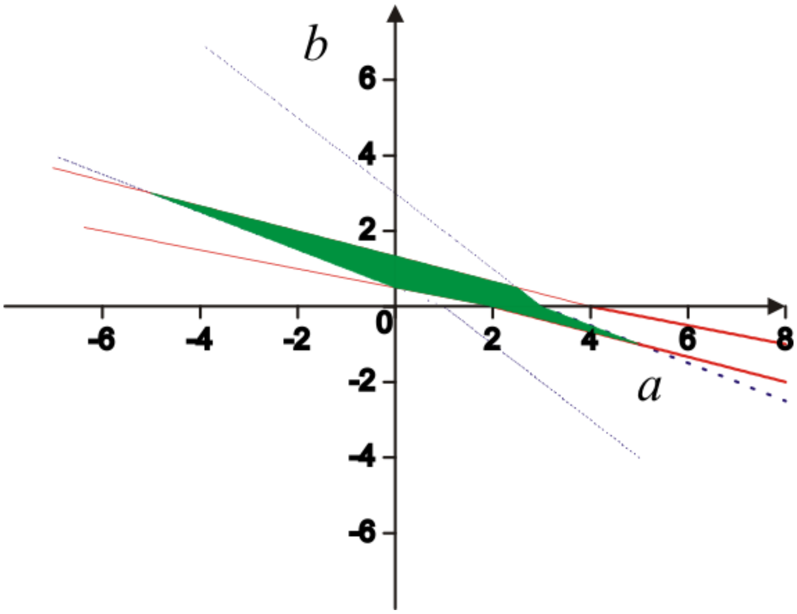

Figure 6-8: A concave feasible region.

6.6. Interval analysis: non-thermodynamic examples

Kantorovich's idea was initially proposed to solve economic problems, and it has been studied during the past half-century. The difference between interval based estimation and statistical point estimation (i.e., least squares estimates) was compared by Zhilin [55]. The author concluded that the non-statistical estimation performs comparably to statistical point estimation in the case of interval errors and insufficient information on data distributions. In another paper [56], Zhilin put forward a method to find outliers. Moreover, this method was applied to image geometric correction of satellite images. In another study from Spivak [57], experimental data was found to enjoy a better description with interval data because they can be analyzed without any statistical characteristics of the measurements. In addition, he gave an example about the determination of the kinetic constants for olefin dehydrogenation that is based on interval estimation. According to Pomerantsev *et al*. [58-61], experimental data are classified into four types: reliable observations, doubtful outliers, significant boundaries and absolute outliers. The method used to distinguish these types of data was named as a simple interval calculation (SIC). Meanwhile, they suggested that all kinds of errors, such as errors in predictors, errors in response, errors in calibration data, and errors in prediction data, should be included during data analysis. An example of the prediction of gasoline "Octane Rating" was illustrated by applying the SIC method.

Although none of the studies described above can present a sound method to calculate a feasible region of parameters, the understanding of interval and data analysis is quite beneficial and helpful to the present study.

7. Non-statistical description of the excess Gibbs energy of the liquid phase in the Ag-Mg system

This study marks the first application of non-statistical modeling to thermodynamic optimization. The Ag-Mg system is selected again because it was assessed by the CALPHAD technique in the present work. However, only the liquid phase can be analyzed here due to the limitations of non-statistical modeling that were previously explained.

7.1. Analysis of experimental data

The thermodynamic data for the liquid phase are mixing enthalpy measured by Kawakami [20] and activity of Mg measured by Gran *et al*. [12]. Even though they were analyzed in Chapter 2, data analysis in non-statistical modeling is different from traditional analysis. The following two Subsections are good examples to illustrate how to apply a non-statistical treatment to the experimental data.

7.1.1. Enthalpy of mixing measured by Kawakami

Figure 7-1 shows a schematic diagram of the Calvet-type calorimeter that was used in Kawakami's experiment. In order to achieve a better evaluation of experimental data, the experimental procedure should be fully understood. At the very beginning, Ag was placed in crucible A and Mg was placed in the tube container B. When the temperature of the furnace reached the required temperature (i.e., T=1323 K), both Ag and Mg melted. After remaining for sufficient time, the porcelain tube D was moved to let the molten Mg fall into the crucible A to mix with the molten Ag. The temperature variation was measured by a thermo-couple.

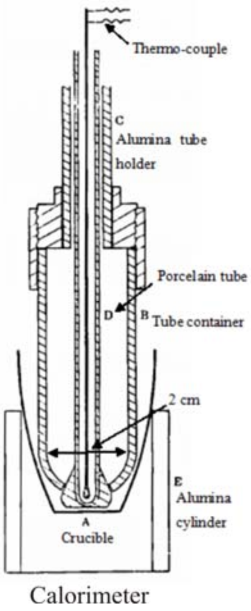

Figure 7-1: A schematic diagram of the Calvet-type calorimeter.

The results are graphically shown in Figure 7-2:

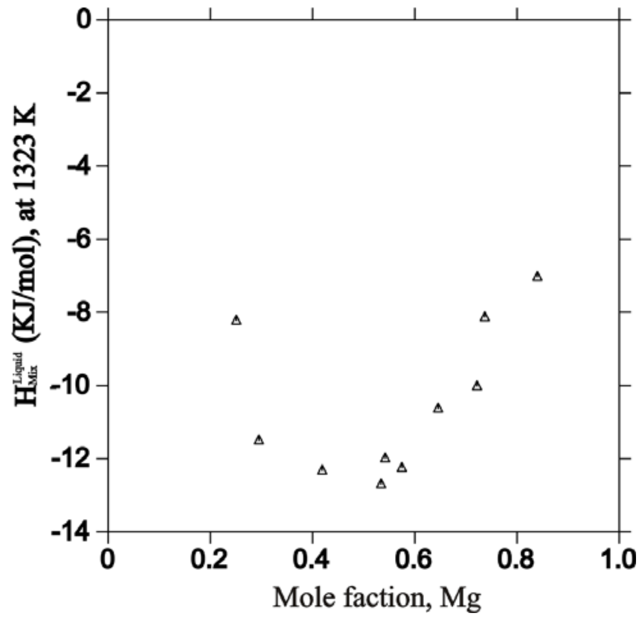

Figure 7-2: Mixing enthalpy in liquid Ag-Mg alloys.

In order to assign reasonable intervals to all experimental data, we need make use of all available information. During sample preparation, there may have been some errors in samples' weights because the weight balance is not absolutely accurate, and its accuracy was ±0.02 g. As for the uncertainty of the temperature, it was affected by two aspects: before mixing the two metals, the accuracy of the thermo-couple was ±5 °C; after the mixing, some heat was released, and the temperature variation was detected by the thermo-couple, but its accuracy would be ±10 ℃ because it may not be very sensitive to the temperature change. The mixing enthalpy was calculated by using the information of the calorimeter, i.e., its heat capacity whose accuracy was assumed to be about ±10%. The uncertainties discussed above are random errors, but in order to provide an interval that contains all possible data, the systematic errors should also be included. Mg is easy to oxidize and volatilize, and this problem would become even worse at higher temperatures. During the experiment, the temperature could be as high as 1323 K. Thus, some amount of Mg was lost, which potentially caused the measured heat to be less than the real heat, and this loss was assumed as 5%.

Even though the uncertainties in experimental conditions were analyzed, they cannot be taken into account due to the limitations explained in Subsection 6.5.3. Figure 7-3 shows the data in a description of intervals.

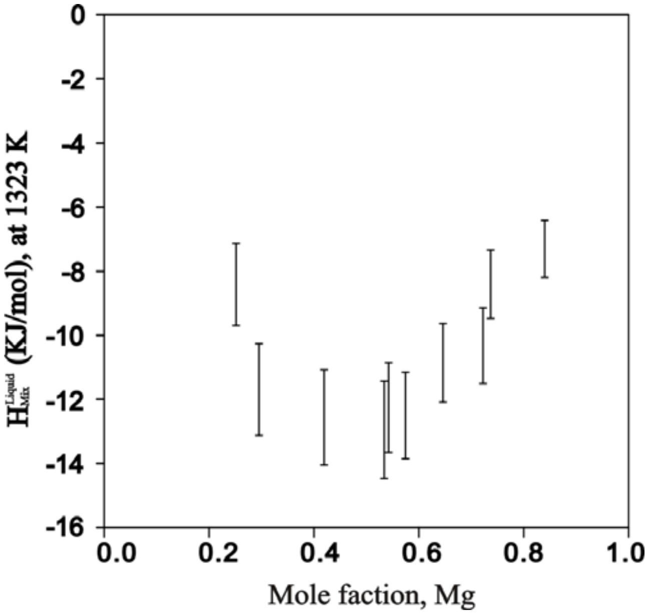

Figure 7-3: Mixing enthalpy in intervals at 1323 K.

7.1.2. Activity of Mg measured by Gran, Song and Sichen

In order to obtain a realistic estimation of uncertainty, we should be fully aware of the experimental process. According to [12], there are two techniques to measure the activity of Mg. The first one is the vapor pressure method, as shown in Figure 7-4. During the experiment, the molten Mg was heated at a high temperature where Mg was evaporated and dissolved in the molten Ag, and its vapor pressure can be calculated by Eq. (7.1):

$$\log_{10} P_{\mathrm{Mg}}(\mathrm{bar}) = 10.7 - \frac{7626}{T(\mathrm{K})} - 1.63 \times \log_{10} T(\mathrm{K}). \tag{7.1}$$

This process would reach equilibrium after remaining for enough time. In addition, Mg and Ag mixed homogeneously to liquid at very high temperature. After cooling, the mixture was analyzed by ICP-AES analysis (Inductively Coupled Plasma-Atomic Emission Spectrometry) to obtain the chemical composition.

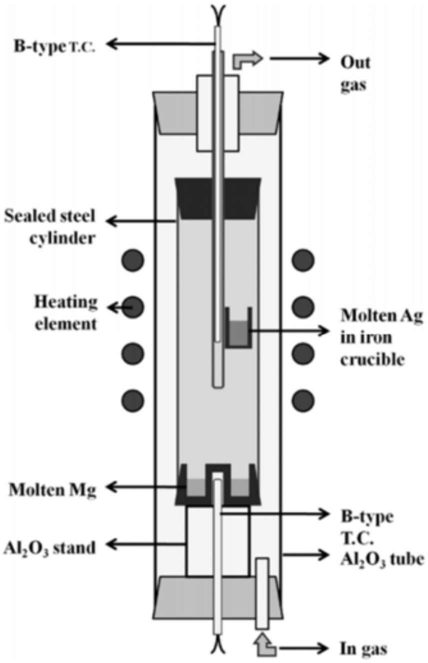

Figure 7-4: The setup used in the vapor pressure method.

Figure 7-5 shows the equipment used in the second technique, which is a gas equilibrium technique. In this experiment, the vapor pressure of Mg was not only monitored by the temperature, but also regulated by the pressure of CO. Finally, the chemical composition of the sample was also characterized by ICP-AES analysis.

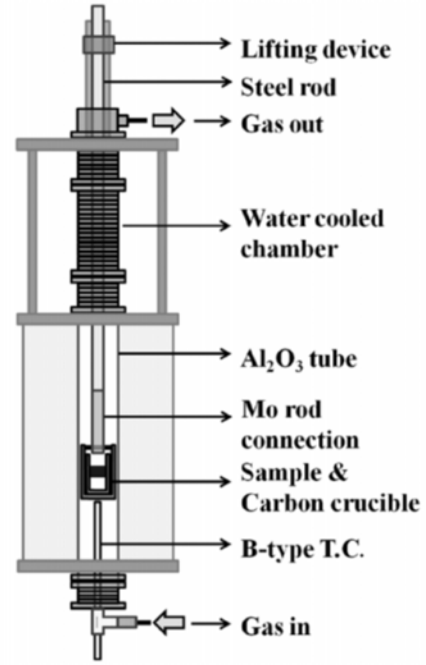

Figure 7-5: The setup used in the gas equilibrium technique.

The activity of Mg was calculated by Eq. (7.2):

$$a_{\mathrm{Mg}} = \frac{P_{\mathrm{Mg}}}{P_{\mathrm{Mg}}^{0}}, \tag{7.2}$$

where P_{Mg} is the pressure of Mg in Ag-Mg melt that was obtained by the pressure formulas described above, and P_{Mg}^{0} is the saturated vapor pressure of Mg that was calculated by:

$$\log_{10} P_{\mathrm{Mg}}^{0}(\mathrm{atm}) = 4.928 - \frac{6778}{T(\mathrm{K})}. \tag{7.3}$$

For the convenience of calculation, the activity of Mg is converted into the excess chemical potential of Mg in the liquid phase:

$${}^{\mathrm{ex}}\mu_{\mathrm{Mg}}^{\mathrm{Liquid}} = \mathrm{R}T\ln\left(\frac{a_{Mg}}{x_{Mg}}\right), \tag{7.4}$$

where x_{Mg} is the measured chemical composition. Figure 7-6 shows the original data from the paper.

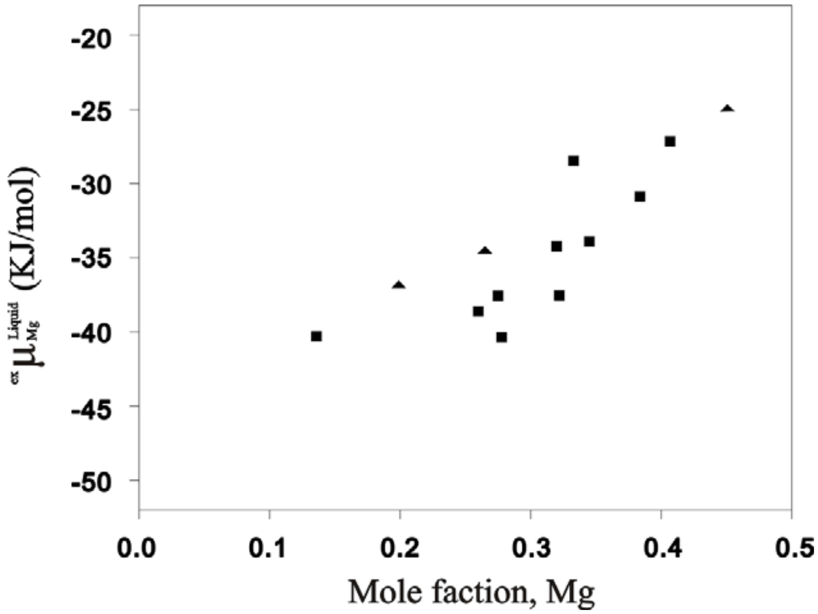

Figure 7-6: Excess chemical potential of Mg in the liquid phase: ■ at 1673 K, ▲ at 1573 K [12].

After that, we will determine the intervals of $^{ex}\mu_{Mg}^{Liquid}$. According to the information from [12], the uncertainty of the temperature was proposed as ±10 K, and the uncertainty of the chemical composition was assumed to be ±10%. As introduced above, the activity of Mg was calculated by combining those two pressure equations: Eq. (7.1) and Eq. (7.3). Thus it is necessary to consider the accuracy of the pressure equations. Unfortunately, there is no available information about uncertainty analysis for these empirical equations. In this case, we compared their calculations with available experimental data to estimate an approximate uncertainty as ±10%. Finally, Figure 7-7 shows the data in a description of intervals.

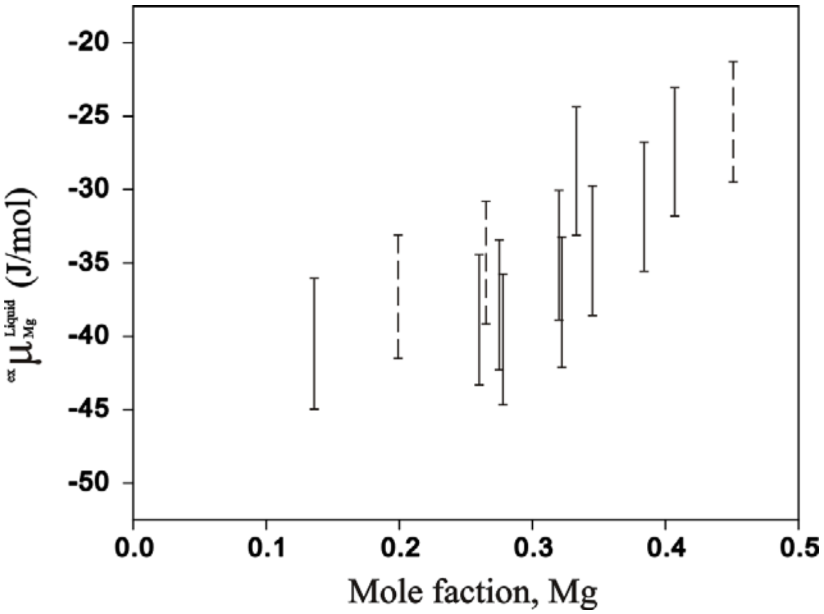

Figure 7-7: The excess chemical potential of Mg in the liquid phase, where the solid intervals are at 1673 K, and dashed intervals are at 1573 K.

7.2. Choosing a suitable model or formalism for the liquid phase

The basic criteria for a good model were discussed in Chapter 3, but they cannot help us to determine the exact number of parameters in a model. In this case, we can only decide which type of the model is most appropriate.

In previous assessments of the Ag-Mg system, the substitutional-regular-solution model was used to simulate the data in the liquid phase. The difference among these assessments, including the assessment of the present work, is the description of the excess Gibbs energy. A general formula was presented by Eq. (3.2).

7.3. Finding feasible regions of interaction parameters for various excess Gibbs energy models

One of the advantages of non-statistical modeling is its ability to judge whether or not a model is satisfactory. Thus we can apply this method to different descriptions of the excess Gibbs energy model to find the most acceptable one.

Let us start with the simplest case where only one parameter A_0 is chosen:

$$^{\mathrm{ex}}G_{\mathrm{AgMg}}^{\mathrm{Liq}} = x_{\mathrm{Ag}} x_{\mathrm{Mg}} \times A_0. \tag{7.5}$$

Thus, the functions for mixing enthalpy and excess chemical potential of Mg are Eq. (7.6) and Eq. (7.7) respectively.

$$\begin{aligned} ^{\mathrm{mix}}H_{\mathrm{AgMg}}^{\mathrm{Liq}} &= {}^{\mathrm{mix}}G_{\mathrm{AgMg}}^{\mathrm{Liq}} - \frac{\partial\, ^{\mathrm{mix}}G_{\mathrm{AgMg}}^{\mathrm{Liq}}}{\partial T} \times T \\ &= x_{\mathrm{Ag}} x_{\mathrm{Mg}} \times A_0, \end{aligned} \tag{7.6}$$

and

$$\begin{aligned} {}^{\mathrm{ex}}\mu_{\mathrm{Mg}}^{\mathrm{Liq}} &= {}^{\mathrm{ex}}G_{\mathrm{AgMg}}^{\mathrm{Liq}} + (1-x_{\mathrm{Mg}})\frac{\partial\,{}^{\mathrm{ex}}G_{\mathrm{AgMg}}^{\mathrm{Liq}}}{\partial x_{\mathrm{Mg}}} \\ &= (1-x_{\mathrm{Mg}})^2 A_0. \end{aligned} \tag{7.7}$$

Feasible values of parameter A_0 can be obtained if it satisfies the following inequalities (7.8) and (7.9):

$$\left(\underline{{}^{\mathrm{mix}}H_{\mathrm{AgMg}}^{\mathrm{Liq}}}_{\mathrm{lower}}\right)_i \le \left(x_{\mathrm{Ag}} x_{\mathrm{Mg}} \times A_0\right)_i \le \left(\overline{{}^{\mathrm{mix}}H_{\mathrm{AgMg}}^{\mathrm{Liq}}}^{\mathrm{upper}}\right)_i, \tag{7.8}$$

and

$$\left(\underline{{}^{\mathrm{ex}}\mu_{\mathrm{Mg}}^{\mathrm{L}}}_{\mathrm{lower}}\right)_j \le \left((1-x_{\mathrm{Mg}})^2 A_0\right)_j \le \left(\overline{{}^{\mathrm{ex}}\mu_{\mathrm{Mg}}^{\mathrm{L}}}^{\mathrm{upper}}\right)_j, \tag{7.9}$$

where *i* and *j* are the number of experimental data for each measurement.

The result of the program shows no feasible region after calculating inequalities (7.8) and (7.9). The reasons for this result of no feasible region may come from three aspects: first, the selected model is not good enough to simulate experimental data; second, the ranges of some intervals are too small to cover all possible data; third, the existence of outliers. According to the analysis of data, the last two reasons are less possible than the first one. Thus, it is recommended to select another model to test.

In addition to the parameter A_0, a composition-dependent parameter A_1 is introduced to the model:

$$ {}^{\mathrm{ex}}G_{\mathrm{AgMg}}^{\mathrm{Liq}} = x_{\mathrm{Ag}} x_{\mathrm{Mg}} \left(A_0 + \left(x_{\mathrm{Ag}} - x_{\mathrm{Mg}} \right) A_1 \right). \tag{7.10} $$

Again, we have the following inequalities after derivation:

$$ \left(\underline{{}^{\mathrm{mix}}H_{\mathrm{AgMg}}^{\mathrm{Liq}}}_{\mathrm{lower}} \right)_i \le \left(x_{\mathrm{Ag}} x_{\mathrm{Mg}} \left(A_0 + \left(x_{\mathrm{Ag}} - x_{\mathrm{Mg}} \right) A_1 \right) \right)_i \le \left(\overline{{}^{\mathrm{mix}}H_{\mathrm{AgMg}}^{\mathrm{Liq}}}^{\mathrm{upper}} \right)_i , \tag{7.11} $$

and

$$ \left(\underline{{}^{\mathrm{ex}}\mu_{\mathrm{Mg}}^{\mathrm{Liq}}}_{\mathrm{lower}} \right)_j \le \left((1 - x_{\mathrm{Mg}})^2 \left(A_0 + \left(1 - 4x_{\mathrm{Mg}} \right) A_1 \right) \right)_j \le \left(\overline{{}^{\mathrm{ex}}\mu_{\mathrm{Mg}}^{\mathrm{Liq}}}^{\mathrm{upper}} \right)_j . \tag{7.12} $$

After the calculation, Figure 7-8 and Figure 7-9 show two feasible regions calculated from inequalities (7.11) and (7.12) respectively.

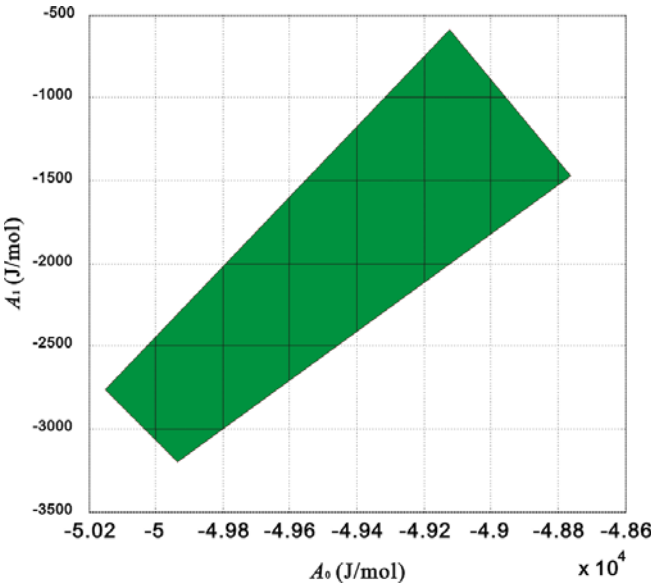

Figure 7-8: A feasible region of parameters A_0 and A_1 based on Kawakami's data.

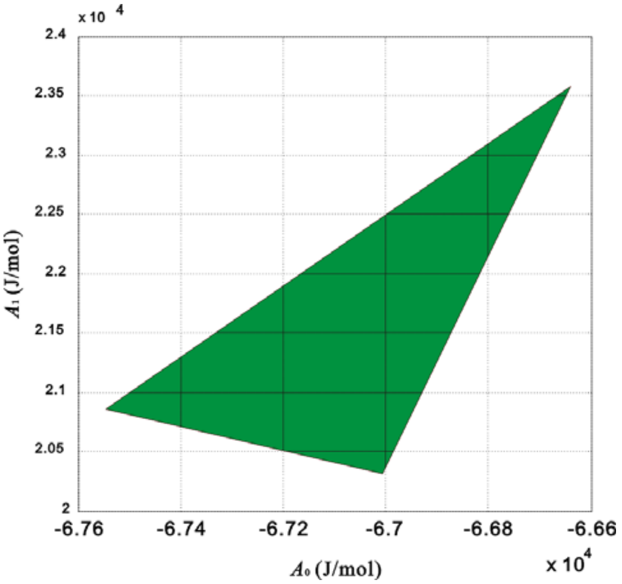

Figure 7-9: A feasible region of parameters A_0 and A_1 based on Gran's data.

We need to compare the two feasible regions to find the overlapping region where all inequalities are satisfied. Apparently, there is no intersection between the two feasible regions (Figure 7-10), which means we still have to test another model.

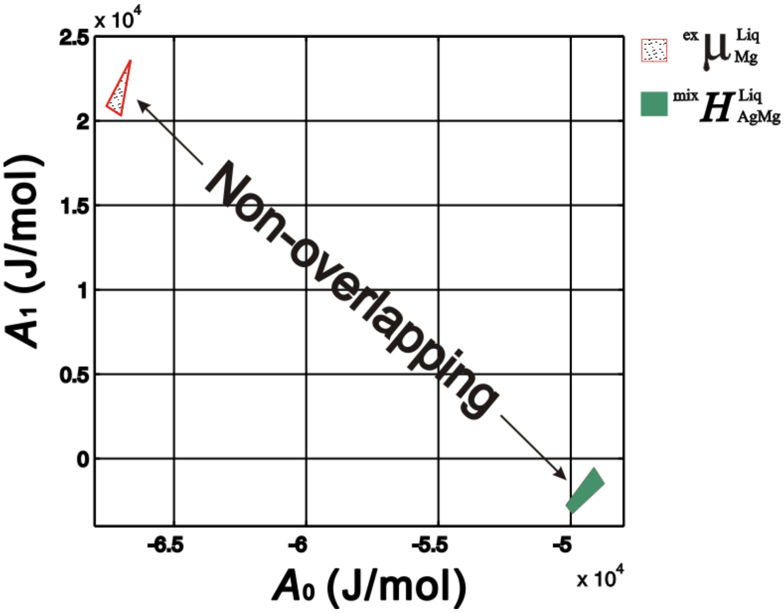

Figure 7-10: The two feasible regions have no overlapping area.

The excess Gibbs energy can also be temperature dependent, but it is worth noting that the mixing enthalpy is independent of temperature if the excess Gibbs energy is linear to temperature. Thus, there is no need to consider a case where the model is:

$$^{\text{ex}}G^{\text{Liq}}_{\text{AgMg}} = x_{\text{Ag}}x_{\text{Mg}}\left(A_0 + B_0 \times T\right). \tag{7.13}$$

Its derivation to the mixing enthalpy is the same as Eq. (7.6) that was confirmed that no feasible region exists. In addition, for the model of Eqs. (7.14) and (7.15), their derivations to the mixing enthalpy are the same as Eq. (7.11), which means that its feasible region of A_0 and A_1 is the same as it shown in Figure 7-8, and it does not care about B_0 that can be any value. However, the descriptions of the excess chemical potential of Mg should be changed, and they are expressed by inequalities (7.16) and (7.17) that correspond to Eqs. (7.14) and (7.15) respectively.

$$^{\text{ex}}G_{\text{AgMg}}^{\text{Liq}} = x_{\text{Ag}}x_{\text{Mg}}\left(\left(A_0 + B_0 \times T\right) + \left(1 - 2x_{\text{Mg}}\right)A_1\right), \tag{7.14}$$

$$^{\text{ex}}G_{\text{AgMg}}^{\text{Liq}} = x_{\text{Ag}}x_{\text{Mg}}\left(A_0 + \left(1 - 2x_{\text{Mg}}\right)\left(A_1 + B_1 \times T\right)\right). \tag{7.15}$$

$$\left(\frac{^{\text{ex}}\mu_{\text{Mg}}^{\text{Liq}}}{\text{lower}}\right)_j \le \left((1 - x_{\text{Mg}})^2\left(\left(A_0 + B_0 \times T\right) + \left(1 - 4x_{\text{Mg}}\right)A_1\right)\right)_j \le \left(\frac{\text{upper}}{^{\text{ex}}\mu_{\text{Mg}}^{\text{Liq}}}\right)_j, \tag{7.16}$$

$$\left(\frac{^{\text{ex}}\mu_{\text{Mg}}^{\text{Liq}}}{\text{lower}}\right)_j \le \left((1 - x_{\text{Mg}})^2\left(A_0 + \left(1 - 4x_{\text{Mg}}\right)\left(A_1 + B_1 \times T\right)\right)\right)_j \le \left(\frac{\text{upper}}{^{\text{ex}}\mu_{\text{Mg}}^{\text{Liq}}}\right)_j. \tag{7.17}$$

Figure 7-11 and Figure 7-12 display the feasible regions by separately solving inequalities (7.16) and (7.17). Comparing the feasible regions between Figure 7-8 and Figure 7-11tells us that the value of A_1 is always positive in Figure 7-11 but is negative in Figure 7-8. Thus there is no intersection for this model (i.e., Eq. (7.14)). Although the values of

A_1 can be negative in Figure 7-12, the values of A_0 are a little lower than that in Figure 7-8.

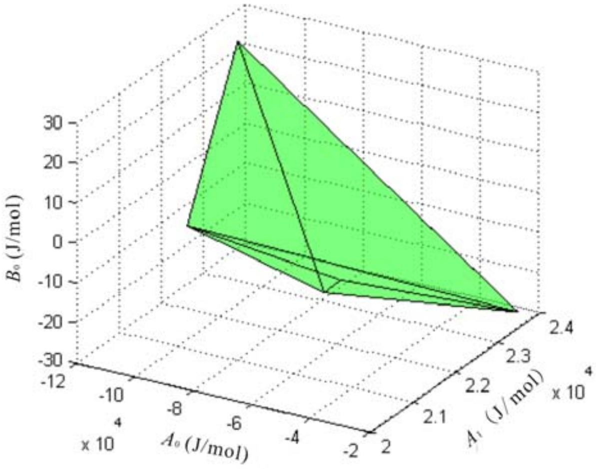

Figure 7-11: A feasible region of parameters A_0, A_1 and B_0 based on Gran's data.

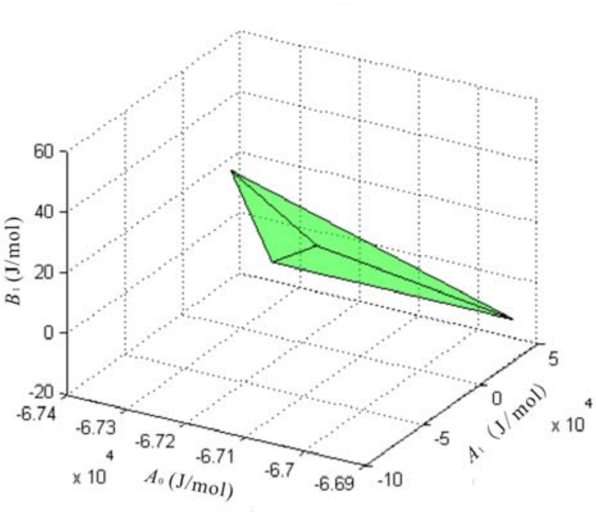

Figure 7-12: A feasible region of parameters A_0, A_1 and B_1 based on Gran's data.

As a result, a good model may exist by combining the two models above. Eq. (7.18) contains four unknown parameters, which could enhance its ability to simulate Gran's data better.

$$ {}^{\mathrm{ex}}G^{\mathrm{Liq}}_{\mathrm{AgMg}} = x_{\mathrm{Ag}} x_{\mathrm{Mg}} \left(\left(A_0 + B_0 \times T \right) + \left(1 - 2x_{\mathrm{Mg}} \right) \left(A_1 + B_1 \times T \right) \right). \tag{7.18} $$

Therefore, a feasible region may exist if inequalities in Eq. (7.19) are all satisfied.

$$ \left(\underline{{}^{\mathrm{ex}}\mu^{\mathrm{Liq}}_{\mathrm{Mg}}}_{\mathrm{lower}} \right)_j \le \left((1 - x_{\mathrm{Mg}})^2 \left(\left(A_0 + B_0 \times T \right) + \left(1 - 4x_{\mathrm{Mg}} \right) \left(A_1 + B_1 \times T \right) \right) \right)_j \le \left(\overline{{}^{\mathrm{ex}}\mu^{\mathrm{Liq}}_{\mathrm{Mg}}}^{\mathrm{upper}} \right)_j \tag{7.19} $$

According to the result of the program, a feasible region was obtained by solving the inequalities of Eq (7.19). However, it is difficult to visualize because it is a four dimensional polytope. Figure 7-13 is an imaginary sketch showing how two feasible regions overlap. Even though the overlapping area cannot be graphically described, the program is able to identify whether or not a point belongs to the region. Moreover, a very important feature of the program is that it can calculate all extreme vertices of a feasible region. As explained above, the feasible values of B_0 and B_1 were only constrained by inequalities (7.19) because the model is linear to temperature. Nevertheless, the feasible values of A_0 and A_1 were limited by both inequalities (7.11) and (7.19). The strategy to find feasible values in the overlap is as follows: first, B_0 and B_1 were fixed by using the information of the extreme vertices; then various values of A_0 and A_1 from the feasible region of Figure 7-8 were tested by the program to examine if they also belong to the 4-D feasible region. Through trial and error, we have found five sets of parameters that are feasible for both Kawakami's and Gran's data, and they are reported in Table 7-1.

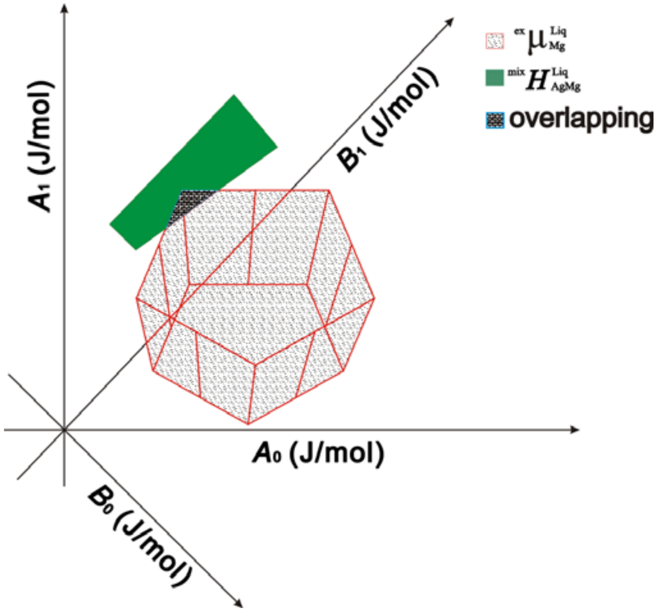

Figure 7-13: A sketched 4-D overlapping feasible region.

Table 7-1: Possible sets of parameters of A_0, A_1, B_0 and B_1.

Parameter	Feasible values (J/mol)				
A_0	-49700	-49800	-49900	-50000	-50100
A_1	[-1900, -1810]	[-2850, -2200]	[-3150, -2300]	[-3050, -2450]	[-2800, -2650]
B_0	-10.24	-10.24	-10.24	-10.24	-10.24
B_1	14.26	14.26	14.26	14.26	14.26

In order to prove the feasibility of the values reported in Table 7-1, we can compare their calculations with the experimental data. A set of parameters was randomly selected and substituted into Eq. (7.18), where $A_0 = -49700$, $A_1 = -1810$, $B_0 = -10.24$ and $B_1 = 14.26$. Then we have:

$$ {}^{\mathrm{ex}}G^{\mathrm{L}}_{\mathrm{AgMg}} = x_{\mathrm{Ag}}x_{\mathrm{Mg}}\left(\left(-49700-10.24\times T\right)+\left(1-2x_{\mathrm{Mg}}\right)\left(-1810+14.26\times T\right)\right). \quad (7.20) $$

Thus, the mixing enthalpy and excess chemical potential of Mg are described as Eqs. (7.21) and (7.22) respectively:

$$ {}^{\mathrm{mix}}H^{\mathrm{Liq}}_{\mathrm{AgMg}} = x_{\mathrm{Ag}}x_{\mathrm{Mg}}\left(-49700-1810\left(1-2x_{\mathrm{Mg}}\right)\right), \quad (7.21) $$

and

$$ {}^{\mathrm{ex}}\mu^{\mathrm{Liq}}_{\mathrm{Mg}} = (1-x_{\mathrm{Mg}})^2\left(\left(-49700-10.24\times T\right)+\left(1-4x_{\mathrm{Mg}}\right)\left(-1810+14.26\times T\right)\right). \quad (7.22) $$

Figure 7-14 shows the calculation of Eq. (7.21) with intervals of mixing enthalpy, and the calculation crosses through all intervals.

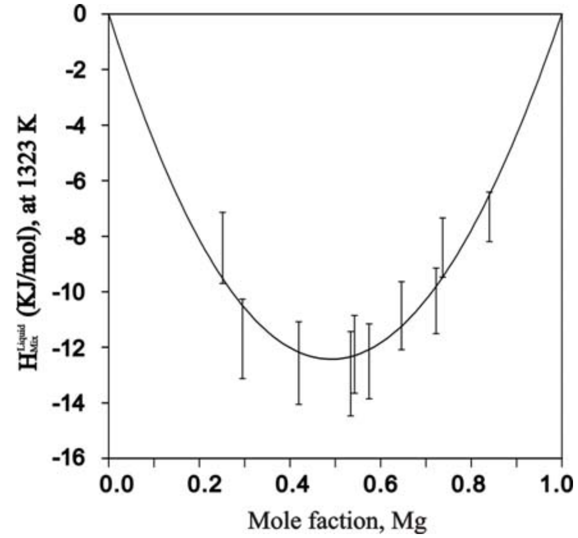

Figure 7-14: The calculated mixing enthalpy at 1323 K, compared with estimated intervals.

Figure 7-15 shows the calculation of Eq. (7.22) with intervals from excess chemical potential of Mg. The solid line was calculated at 1673 K, and it crosses through all intervals that were measured at 1673 K. The dashed line was calculated at 1573 K, and it also crosses through all intervals that measured at 1573 K.

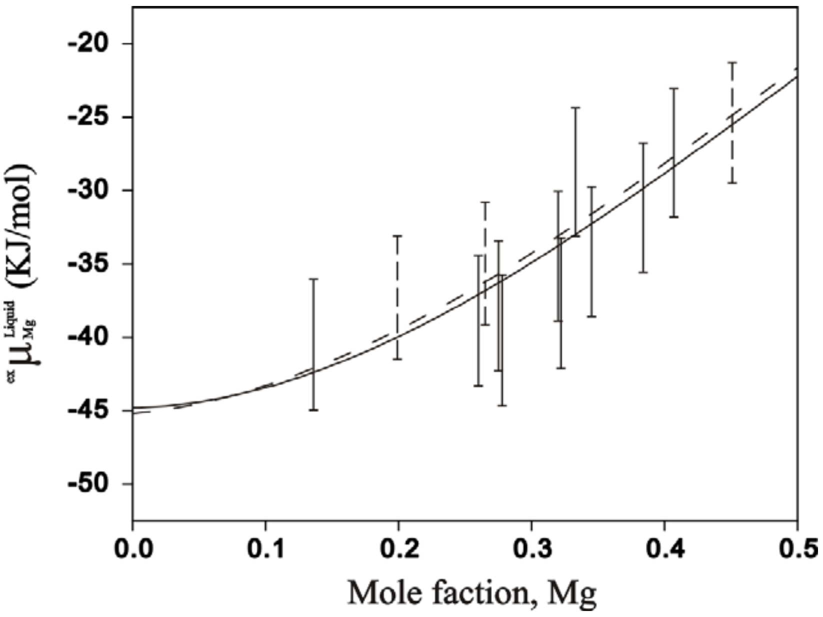

Figure 7-15: The calculated excess chemical potential of Mg, compared with estimated intervals; the solid line is calculated at 1673 K, and the dashed line is calculated at 1573 K.

Therefore, a four-parameter substitutional-solution model is recommended to describe the liquid phase of the Ag-Mg system by using non-statistical modeling. Although it is likely that a feasible region can also be obtained if more parameters are included, it is not a good idea to use many parameters on the liquid phase of a binary system.

7.4. Inapplicability of the interval approach for a full-fledged thermodynamic optimization

During the study of this method, we found that there are too many difficulties to deal with. The three most difficult problems were described in Section 6.5, and they are very common in thermodynamic optimization.

First, it is natural and important to consider uncertainties in experimental conditions, but it is not allowed in the interval approach. Even if they are set to zero, the model is usually non-linear to parameters when it is used to describe data that is measured in the mixtures or phase diagram data, and a non-linear model cannot be solved by the interval approach. Moreover, some phases may require many parameters due to complicated transitions, and thus it would be a problem to visualize a high-dimensional feasible region. Last but not least, the sub-lattice model cannot be used in the interval approach because the site fractions cannot be calculated.

7.5. Using the interval approach as a pre-optimization tool for detecting incompatible sets of experimental data, identifying outliers within individual sets and finding initial approximations

Even though a full-fledged thermodynamic optimization cannot be fulfilled by the interval approach alone, it can be treated as a pre-optimization tool for the traditional CALPHAD technique. In other words, the interval approach plays a role in thermodynamic optimization if the data is measured in a single phase and the model is relatively simple, such as a substitutional-solution model.

One of advantages of the interval approach is its ability to detect incompatible sets of experimental data. The different sets of data are first solved by the interval approach separately to calculate a feasible region for each set, and in an ideal case, an overlap is obtained from them. However, an overlap might not exist due to the reasons discussed in section 7.3. If we are very confident about the selected model and the assigned uncertainties, then it is possible that there are at least two conflicting data that can be determined by the area of the feasible region.

Another benefit of the interval approach is its ability to detect outliers with individual sets. If outliers are not removed before the calculation, then it is very likely that there is no feasible region. Furthermore, it means that some inequalities are not satisfied, and they correspond to the intervals that have no intersection with the calculation of the model. The method of finding outliers is to gradually expand the range of the intervals until the calculation crosses through all intervals. More discussion about this method can be found in [55,56].

As mentioned in Subsection 4.1.2, it is always troublesome to determine initial values of unknown parameters in the traditional CALPHAD technique. However, through the interval approach, any points in a feasible region of parameters are good initial values of unknown parameters.

Conclusions

The present thesis was set out to re-assess the Ag-Mg system using the CALPHAD technique and has obtained a good agreement between calculated and experimental data. The results suggest that a four-sublattice model is employed to model a first-order transition between the FCC and the $L1_2$ phase, and a two-sublattice model is used to simulate a second-order transition in the same phase. It is however, noted from the discussion of the CALPHAD technique that the deficiencies of this technique should not be ignored.

The interval approach provides an alternative idea for thermodynamic optimization, and it overcomes the shortcomings of the CALPHAD technique: reasonable uncertainties can be estimated without statistical calculation; the number of unknown parameters for substitutional-solution model can be approximately identified; good initial values of unknown parameters can be determined from a feasible region if it exists; and outliers can be found if a feasible region does not exist. However, throughout the study, we also found that this method is limited to particular problems.

For the CALPHAD technique and the interval approach, it is not recommended to judge that one method is better than the other because their respective advantages exist in particular situations. Thus, a promising approach is to comprehensively combine both of them for thermodynamic optimization.

Appendix I

Phase Diagram Data

Phase		at% Mg	at% ΔMg	Temp (K)	ΔTemp (K)	Weight	References
Liquid $\rightleftarrows$ $HCP+AgMg_3$	HCP	96.00	0.10	745.00	1.00	1.5	Lim *et al.* [21]
	Liquid	82.00	0.10				
	$AgMg_3$	77.00	0.10				
$AgMg_3$ $\rightleftarrows$ Liquid+B2_BCC	$AgMg_3$	77.00	0.10	764.00	1.00		
	B2_BCC	65.00	0.10				
	Liquid	77.00	0.10				
$AgMg_4$ $\rightleftarrows$ $HCP+AgMg_3$	HCP	96.00	0.10	742.00	1.00		
	$AgMg_4$	80.00	0.10				
	$AgMg_3$	77.00	0.10				
$AgMg_3$ $\rightleftarrows$ Liquid+B2_BCC	B2_BCC	65.43	0.50	765.15	0.50		Żemczużnyj [23]
	Liquid	77.43	0.50				
	$AgMg_3$	77.00	0.50				
Liquid $\rightleftarrows$ $AgMg_3+HCP$	HCP	96.00	0.50	742.15	0.50	0.5	
	Liquid	82.70	0.50				
	$AgMg_3$	77.00	0.50				
Liquid $\rightleftarrows$ $L1_2$+B2_BCC	Liquid	50.00	0.50	1093.15	0.5	1.5	
	B2_BCC	50.00	0.50				
Liquid $\rightleftarrows$ $L1_2$+B2_BCC	$L1_2$	0.2815	0.50	1029.15	0.5		
	Liquid	0.3410	0.50				
	B2_BCC	0.3740	0.50				
Liquid $\rightleftarrows$ $L1_2$+B2_BCC	$L1_2$	29.3	0.40	1032.45	0.40		Andrews *et al.* [25]
	Liquid	33.40	0.20				
	B2_BCC	35.5	0.40				
Liquid $\rightleftarrows$ $HCP+AgMg_3$	HCP	96.10	0.10	744.15	1.50		Hume-Rothery *et al.* [22]
	Liquid	82.00	0.10				
	$AgMg_3$	77.00	0.10				
Liquid $\rightleftarrows$ $HCP+AgMg_3$	HCP	96.10	0.20	745.15	2.00		Payne *et al.* [24]
	Liquid	82.44	0.20				
	$AgMg_3$	77.00	0.20				
$AgMg_4$ $\rightleftarrows$	HCP	96.00	0.82	738.15	2.00		Kolesnichenko *et al.*

	$AgMg_3$	77.00	0.82				[27]
	$AgMg_4$	80.00	0.82				
Liquidus: Liquid & FCC		33.28	0.50	1039.15	0.50	1	Żemcżużnyj [23]
		32.37	0.50	1047.15	0.50		
		32.25	0.50	1048.15	0.50		
		31.70	0.50	1053.65	0.50		
		30.20	0.50	1059.65	0.50		
		29.50	0.50	1065.15	0.50		
		29.23	0.50	1066.15	0.50		
		28.90	0.50	1068.15	0.50		
		28.15	0.50	1076.65	0.50		
		27.10	0.50	1083.65	0.50		
		26.80	0.50	1083.15	0.50		
		26.55	0.50	1087.15	0.50		
		22.06	0.50	1109.65	0.50		
		19.84	0.50	1121.15	0.50		
		15.59	0.50	1145.15	0.50		
		12.35	0.50	1160.65	0.50		
		10.60	0.50	1171.15	0.50		
		7.11	0.50	1188.65	0.50		
		3.03	0.50	1210.65	0.50		
		1.57	0.50	1220.85	0.50		
		1.00	0.50	1227.15	0.50		
Solidus: FCC & Liquid		27.10	0.50	1043.15	0.50		
		26.80	0.50	1043.15	0.50		
		26.55	0.50	1045.15	0.50		
		22.06	0.50	1082.15	0.50		
		19.84	0.50	1095.15	0.50		
		15.59	0.50	1103.15	0.50		
		12.35	0.50	1141.15	0.50		
		10.60	0.50	1153.15	0.50		
		7.11	0.50	1172.15	0.50		
		3.03	0.50	1201.15	0.50		
		1.57	0.50	1211.15	0.50		
Liquidus: Liquid & B2_BCC		48.60	0.50	1091.15	0.50		
		47.56	0.50	1089.65	0.50		
		47.37	0.50	1089.65	0.50		

	44.79	0.50	1082.15	0.50		
	44.65	0.50	1081.15	0.50		
	43.20	0.50	1078.15	0.50		
	43.00	0.50	1076.15	0.50		
	42.80	0.50	1077.15	0.50		
	41.08	0.50	1067.65	0.50		
	40.13	0.50	1061.65	0.50		
	39.58	0.50	1061.15	0.50		
	39.40	0.50	1061.15	0.50		
	39.00	0.50	1055.65	0.50		
	38.40	0.50	1053.15	0.50		
	37.40	0.50	1048.15	0.50		
	37.10	0.50	1044.15	0.50		
	35.40	0.50	1036.15	0.50		
	35.20	0.50	1035.15	0.50		
	34.60	0.50	1031.65	0.50		
	76.65	0.50	779.65	0.50		
	75.70	0.50	800.65	0.50		
	75.00	0.50	805.65	0.50		
	74.80	0.50	811.15	0.50		
	72.02	0.50	871.65	0.50		
	69.32	0.50	923.15	0.50		
	69.00	0.50	923.15	0.50		
	68.50	0.50	943.15	0.50		
	66.80	0.50	965.15	0.50		
	66.04	0.50	982.65	0.50		
	65.43	0.50	989.15	0.50		
	64.64	0.50	1005.15	0.50		
	64.30	0.50	1005.15	0.50		
	63.20	0.50	1019.15	0.50		
	62.25	0.50	1028.65	0.50		
	60.38	0.50	1055.15	0.50		
	58.68	0.50	1068.15	0.50		
	56.55	0.50	1080.15	0.50		
	55.40	0.50	1083.15	0.50		
	54.68	0.50	1085.15	0.50		
	52.70	0.50	1088.65	0.50		

	51.70	0.50	1090.65	0.50		
Solidus: B2_BCC & Liquid	62.25	0.50	945.15	0.50		
	60.38	0.50	993.15	0.50		
	58.68	0.50	1031.15	0.50		
	56.55	0.50	1058.15	0.50		
	55.40	0.50	1069.15	0.50		
	54.68	0.50	1071.15	0.50		
	52.70	0.50	1081.15	0.50		
	51.70	0.50	1087.15	0.50		
	48.60	0.50	1086.15	0.50		
	47.56	0.50	1079.15	0.50		
	47.37	0.50	1078.15	0.50		
	44.79	0.50	1063.15	0.50		
	44.65	0.50	1065.15	0.50		
	43.20	0.50	1059.15	0.50		
	43.00	0.50	1056.15	0.50		
	42.80	0.50	1056.15	0.50		
	41.08	0.50	1045.15	0.50		
	40.13	0.50	1041.15	0.50		
	39.58	0.50	1041.15	0.50		
	39.40	0.50	1039.15	0.50		
	39.00	0.50	1035.15	0.50		
	38.40	0.50	1035.65	0.50		
Liquidus: Liquid & $AgMg_3$	82.47	0.50	746.15	0.50		
	81.60	0.50	751.15	0.50		
	79.49	0.50	760.15	0.50		
	79.10	0.50	759.65	0.50		
Liquidus: Liquid & HCP	99.00	0.50	922.15	0.50		
	97.56	0.50	904.65	0.50		
	93.60	0.50	874.15	0.50		
	90.65	0.50	839.15	0.50		
	85.30	0.50	766.65	0.50		
B2_BCC & $L1_2$	27.20	0.27	613.85	3.00	1	Kachi [29]
	27.20	0.27	633.96	3.00		
	27.20	0.27	647.35	3.00		
	27.20	0.27	663.28	3.00		
	27.20	0.27	613.83	3.00		

	27.20	0.27	623.88	3.00		
	27.20	0.27	633.94	3.00		
	27.20	0.27	644.83	3.00		
	27.20	0.27	654.88	3.00		
	27.20	0.27	663.26	3.00		
B2_BCC & FCC	27.20	0.27	694.27	3.00		
	27.20	0.27	711.88	3.00		
	27.20	0.27	718.56	3.00		
	27.20	0.27	747.88	3.00		
	27.20	0.27	762.96	3.00		
	27.20	0.27	803.17	3.00		
	27.20	0.27	829.95	3.00		
Solidus: FCC & Liquid	6.38	0.40	1177.04	3.00	1	Andrews *et al*. [25]
	13.38	0.40	1126.27	3.00		
	16.67	0.40	1105.64	3.00		
	24.92	0.40	1059.29	3.00		
Liquidus: Liquid & FCC	4.79	0.40	1211.15	0.50		
	9.42	0.40	1187.45	0.50		
	14.18	0.40	1161.25	0.50		
	20.40	0.40	1123.55	0.50		
	23.96	0.40	1100.75	0.50		
	28.63	0.40	1067.55	0.50		
Liquidus: Liquid & B2_BCC	33.84	0.40	1036.15	0.50		
	38.50	0.40	1063.05	0.50		
	39.68	0.40	1071.75	0.50		
FCC	26.40	0.33	728.56	4.00		
	26.80	0.33	832.78	4.00		
	27.10	0.33	912.69	4.00		
	27.20	0.33	1015.15	4.00		
$L1_2$ & B2_BCC	27.60	0.33	569.74	4.00		
	27.40	0.33	644.40	4.00		
FCC & B2_BCC	28.00	0.33	728.67	4.00		
	28.10	0.33	832.87	4.00		
	28.10	0.33	914.49	4.00		
	28.90	0.33	1014.40	4.00		
	36.10	0.33	913.27	4.00		
	36.50	0.33	833.42	4.00		

	37.50	0.33	753.60	4.00		
B2_BCC	36.00	0.33	1009.65	4.00		
	38.10	0.33	975.92	4.00		
	39.00	0.33	754.56	4.00		
	41.20	0.33	568.89	4.00		
Solvus: HCP	99.10	0.01	573.15	1.50	1	Hume-Rothery *et al.* [22]
HCP	99.01	0.08	731.20	2.50		
	98.81	0.08	731.04	2.50		
	97.91	0.08	731.02	2.50		
	97.51	0.08	731.37	2.50		
	96.91	0.08	731.54	2.50		
	96.51	0.08	727.74	2.50		
	96.95	0.08	747.81	2.50		
	96.52	0.08	745.18	2.50		
	96.92	0.08	765.26	2.50		
	97.52	0.08	784.84	2.50		
	97.92	0.08	804.27	2.50		
	99.02	0.08	814.90	2.50		
	98.82	0.08	836.27	2.50		
	99.03	0.08	854.44	2.50		
	99.41	0.08	875.07	2.50		
	96.53	0.08	728.15	2.50		
	96.93	0.08	732.15	2.50		
	97.53	0.08	713.15	2.50		
	97.93	0.08	673.15	2.50		
	98.83	0.08	673.15	2.50		
	99.04	0.08	616.15	2.50		
	99.21	0.08	579.15	2.50		
	99.42	0.08	874.65	2.50		
	99.05	0.08	854.15	2.50		
	98.84	0.08	836.65	2.50		
	97.94	0.08	805.15	2.50		
	97.54	0.08	785.15	2.50		
	96.94	0.08	766.15	2.50		
	96.54	0.08	746.15	2.50		
HCP & $AgMg_4$	99.01	0.08	577.69	2.50		
	98.81	0.08	614.76	2.50		

	97.93	0.08	614.74	2.50		
	97.52	0.08	615.07	2.50		
	96.94	0.08	614.67	2.50		
	96.56	0.08	614.95	2.50		
	95.97	0.08	615.17	2.50		
	95.46	0.08	615.35	2.50		
	94.90	0.08	615.01	2.50		
	97.51	0.08	672.07	2.50		
	96.93	0.08	671.65	2.50		
	96.59	0.08	671.93	2.50		
	96.92	0.08	692.59	2.50		
	96.00	0.08	727.40	2.50		
	95.40	0.08	727.00	2.50		
	94.93	0.08	726.66	2.50		
	96.06	0.08	728.15	2.50		
	96.54	0.08	673.15	2.50		
	96.97	0.08	694.15	2.50		
	97.56	0.08	673.15	2.50		
	97.92	0.08	616.15	2.50		
	98.82	0.08	616.15	2.50		
	99.02	0.08	579.15	2.50		
HCP & Liquid	94.99	0.08	745.26	2.50		
	96.57	0.08	756.22	2.50		
	96.95	0.08	776.30	2.50		
	97.52	0.08	795.32	2.50		
	97.93	0.08	814.15	2.50		
	98.84	0.08	847.90	2.50		
	99.02	0.08	860.25	2.50		
	99.03	0.08	868.39	2.50		
	99.41	0.08	886.13	2.50		
	99.42	0.08	893.09	2.50		
	99.43	0.08	886.15	2.50		
	99.05	0.08	861.65	2.50		
	98.86	0.08	848.65	2.50		
	97.93	0.08	815.15	2.50		
	97.55	0.08	795.65	2.50		
	96.98	0.08	777.15	2.50		

	96.54	0.08	756.65	2.50		
Liquidus: Liquid & HCP	94.76	0.05	878.90	2.00	1	Payne *et al*. [24]
	94.76	0.05	881.15	2.00		
	89.89	0.05	821.65	2.00		
	89.88	0.05	824.64	2.00		
	85.53	0.05	773.72	2.00		
	85.53	0.05	778.22	2.00		
Liquidus: Liquid & $AgMg_3$	81.11	0.05	752.83	2.00		
	81.11	0.05	754.33	2.00		
HCP	99.30	0.06	572.32	2.50		
	98.85	0.06	672.35	2.50		
	98.67	0.06	673.01	2.50		
	98.16	0.06	722.94	2.50		
	97.82	0.06	722.09	2.50		
	97.54	0.06	722.72	2.50		
	97.40	0.06	753.36	2.50		
	98.10	0.06	775.26	2.50		
	97.52	0.06	775.07	2.50		
	98.14	0.06	793.96	2.50		
	98.62	0.06	812.07	2.50		
	99.15	0.06	833.19	2.50		
	99.55	0.06	855.03	2.50		
	99.00	0.06	855.60	2.50		
	99.50	0.06	873.72	2.50		
Liquid & HCP	97.40	0.06	793.73	2.50		
	98.10	0.06	812.64	2.50		
	97.50	0.06	810.93	2.50		
	98.10	0.06	833.58	2.50		
	98.60	0.06	855.43	2.50		
	99.10	0.06	873.55	2.50		
	99.60	0.06	896.91	2.50		
HCP & $AgMg_4$	99.80	0.06	472.33	2.50		
	99.60	0.06	472.24	2.50		
	99.30	0.06	472.14	2.50		
	99.10	0.06	572.99	2.50		
	98.80	0.06	572.90	2.50		
	98.30	0.06	672.16	2.50		

	98.10	0.06	672.84	2.50		
	97.00	0.06	722.57	2.50		
	96.50	0.06	722.39	2.50		
Solvus: HCP	99.88	0.16	473.15	2.50	1	Schürmann *et al.* [26]
	99.20	0.16	574.24	2.50		
	98.09	0.16	672.61	2.50		
$AgMg_4$	80.00	0.16	474.24	2.50	0	
	80.00	0.16	573.69	2.50		
	80.00	0.16	673.69	2.50		
HCP & $AgMg_4$	82.40	2.18	723.15	2.00	1	Kolesnichenko *et al.* [27]
	82.00	2.18	673.15	2.00		
$AgMg_3$ & $AgMg_4$	81.40	2.18	673.15	2.00	0	
	80.35	2.18	673.15	2.00		
	78.50	2.18	673.15	2.00	1	
	80.30	2.18	743.15	2.00	0	
	80.34	2.18	723.15	2.00		
	77.80	2.18	673.15	2.00		
$AgMg_3$ & B2_BCC	70.00	2.18	673.15	2.00	1	
	75.80	2.18	673.15	2.00		
$AgMg_4$	80.00	1.00	673.15	2.00	1	
$AgMg_3$	76.80	2.18	723.15	2.00	0	
	75.80	2.18	757.15	2.00		
	78.20	2.18	720.15	2.00		
FCC	15.45	0.38	499.55	22.96	1	Fujiwara *et al.* [30]
	17.91	0.38	522.74	30.19		
	23.11	0.38	648.37	3.75		
FCC	23.00	0.20	641.74	1.20	1	Buckley *et al.* [31]
	24.30	0.20	652.29	1.20		
	25.50	0.20	662.69	1.20		
FCC	24.30	0.20	628.40	2.00		
	25.50	0.20	641.74	2.00		

Thermodynamic Properties

Phase	at% Mg	at% ΔMg	Temp (K)	ΔTemp (K)	Enthalpy (J/mol)	ΔEnthalpy (J/mol)	Weight	References
Liquid	25.10	0.13	1323.15	15.00	-8236.30	6.589E+02	1	Kawakami [20]
	29.50	0.15	1323.15	15.00	-11517.00	9.214E+02		
	41.90	0.21	1323.15	15.00	-12335.00	9.868E+02		
	53.40	0.27	1323.15	15.00	-12711.00	1.017E+03		
	54.20	0.27	1323.15	15.00	-12004.00	9.604E+02		
	57.50	0.29	1323.15	15.00	-12263.00	9.810E+02		
	64.60	0.32	1323.15	15.00	-10643.00	8.514E+02		
	72.20	0.36	1323.15	15.00	-10032.00	8.026E+02		
	73.70	0.37	1323.15	15.00	-8144.00	6.515E+02		
	84.00	0.42	1323.15	15.00	-7044.30	5.636E+02		

Phase	at% Mg	at% ΔMg	Temp (K)	ΔTemp (K)	Activity (Mg)	ΔActivity (Mg)	Weight	References
Liquid	27.80	2.78	1673.00	5.00	1.530E-02	1.530E-03	1	Gran *et al*. [12]
	27.50	2.75	1673.00	5.00	1.840E-02	1.840E-03		
	13.60	1.36	1673.00	5.00	7.530E-03	7.530E-04		
	33.30	3.33	1673.00	5.00	4.290E-02	4.290E-03		
	40.70	4.07	1673.00	5.00	5.770E-02	5.770E-03		
	32.00	3.20	1673.00	5.00	2.730E-02	2.730E-03		
	38.40	3.84	1673.00	5.00	4.160E-02	4.160E-03		
	26.00	2.60	1673.00	5.00	1.620E-02	1.620E-03		
	32.20	3.22	1673.00	5.00	2.160E-02	2.160E-03		
	34.50	3.45	1673.00	5.00	3.010E-02	3.010E-03		
	45.10	4.51	1573.00	5.00	6.590E-02	6.590E-03		
	26.50	2.65	1573.00	5.00	1.860E-02	1.860E-03		
	19.90	1.99	1573.00	5.00	1.170E-02	1.170E-03		
	0.29	0.03	1773.00	5.00	1.600E-04	1.600E-05		
	0.27	0.03	1773.00	5.00	1.600E-04	1.600E-05		
	0.36	0.04	1823.00	5.00	2.000E-04	2.000E-05		
	0.33	0.03	1823.00	5.00	2.000E-04	2.000E-05		
	0.32	0.03	1823.00	5.00	2.000E-04	2.000E-05		

Phase	at% Mg	at% ΔMg	Temp (K)	ΔTemp (K)	Cp (J/mol*K)	ΔCp (J/mol*K)	Weight	References
B2_BCC	50.00	1.00	373.15	5.00	24.64	2.464E-01	1	Schübel [28]

	50.00	1.00	473.15	5.00	26.07	2.607E-01		
	50.00	1.00	573.15	5.00	26.94	2.695E-01		
	50.00	1.00	673.15	5.00	27.74	2.774E-01		
	50.00	1.00	773.15	5.00	28.83	2.883E-01		
	50.00	1.00	873.15	5.00	29.58	2.958E-01		
Phase	at% Mg	at% ΔMg	Temp (K)	ΔTemp (K)	Mur (J/mol)	ΔMur (J/mol)	Weight	References
B2_BCC	51.52	0.52	633.72	3.00	-5339.66	1.930E+02	1	Kachi [29]
	51.52	0.52	642.96	3.00	-5940.69	1.930E+02		
	51.52	0.52	654.65	3.00	-6218.89	1.930E+02		
	51.52	0.52	669.70	3.00	-6644.07	1.930E+02		
	51.52	0.52	683.08	3.00	-7074.50	1.930E+02		
	51.52	0.52	693.16	3.00	-7830.37	1.930E+02		
	51.52	0.52	702.36	3.00	-8116.45	1.930E+02		
	51.52	0.52	721.59	3.00	-8685.98	1.930E+02		
	51.52	0.52	743.26	3.00	-8775.21	1.930E+02		
	51.52	0.52	749.16	3.00	-9386.73	1.930E+02		
	51.52	0.52	767.59	3.00	-10273.83	1.930E+02		
	51.52	0.52	789.32	3.00	-10835.49	1.930E+02		
	51.52	0.52	799.38	3.00	-11433.89	1.930E+02		
	51.52	0.52	812.80	3.00	-12179.26	1.930E+02		
	49.78	0.50	632.32	3.00	-26457.57	1.930E+02		
	49.78	0.50	683.15	3.00	-25528.73	1.930E+02		
	49.78	0.50	738.15	3.00	-24123.91	1.930E+02		
	49.78	0.50	811.48	3.00	-23279.98	1.930E+02		
	48.97	0.49	631.48	3.00	-35160.04	1.930E+02		
	48.97	0.49	666.48	3.00	-34947.38	1.930E+02		
	48.97	0.49	716.48	3.00	-34711.09	1.930E+02		
	48.97	0.49	807.32	3.00	-34016.66	1.930E+02		
	48.97	0.49	813.15	3.00	-34322.53	1.930E+02		
	48.97	0.49	831.48	3.00	-33821.06	1.930E+02		
	47.00	0.47	622.32	3.00	-35489.54	1.930E+02		
	47.00	0.47	633.98	3.00	-35392.40	1.930E+02		
	47.00	0.47	659.82	3.00	-35509.23	1.930E+02		
	47.00	0.47	662.32	3.00	-35426.53	1.930E+02		
	47.00	0.47	674.82	3.00	-35328.07	1.930E+02		
	47.00	0.47	682.32	3.00	-35158.73	1.930E+02		

	47.00	0.47	689.82	3.00	-35146.92	1.930E+02		
	47.00	0.47	716.48	3.00	-35026.15	1.930E+02		
	47.00	0.47	741.48	3.00	-34829.24	1.930E+02		
	47.00	0.47	759.82	3.00	-34879.12	1.930E+02		
	47.00	0.47	784.82	3.00	-34760.98	1.930E+02		
	47.00	0.47	798.98	3.00	-34817.42	1.930E+02		
	47.00	0.47	816.48	3.00	-34789.86	1.930E+02		
	47.00	0.47	831.48	3.00	-34687.46	1.930E+02		
	44.22	0.44	632.32	3.00	-35867.60	1.930E+02		
	44.22	0.44	672.32	3.00	-35804.59	1.930E+02		
	44.22	0.44	715.65	3.00	-35736.33	1.930E+02		
	44.22	0.44	778.98	3.00	-35400.27	1.930E+02		
	44.22	0.44	818.98	3.00	-35652.32	1.930E+02		
	44.50	0.45	622.32	3.00	-36592.23	1.930E+02		
	44.50	0.45	633.15	3.00	-36575.16	1.930E+02		
	44.50	0.45	658.98	3.00	-36613.23	1.930E+02		
	44.50	0.45	662.32	3.00	-36765.51	1.930E+02		
	44.50	0.45	674.82	3.00	-36509.53	1.930E+02		
	44.50	0.45	688.98	3.00	-36565.97	1.930E+02		
	44.50	0.45	716.48	3.00	-36365.13	1.930E+02		
	44.50	0.45	741.48	3.00	-36325.74	1.930E+02		
	44.50	0.45	758.15	3.00	-36299.49	1.930E+02		
	44.50	0.45	785.65	3.00	-36334.93	1.930E+02		
	44.50	0.45	798.98	3.00	-36156.40	1.930E+02		
	44.50	0.45	816.48	3.00	-36286.36	1.930E+02		
	44.50	0.45	831.48	3.00	-36183.97	1.930E+02		
	43.17	0.43	633.98	3.00	-37440.25	1.930E+02		
	43.17	0.43	665.65	3.00	-37311.60	1.930E+02		
	43.17	0.43	688.98	3.00	-37196.08	1.930E+02		
	43.17	0.43	706.48	3.00	-37089.75	1.930E+02		
	43.17	0.43	738.98	3.00	-37038.55	1.930E+02		
	43.17	0.43	771.48	3.00	-36908.59	1.930E+02		
	43.17	0.43	803.15	3.00	-36858.71	1.930E+02		
	40.02	0.40	633.98	3.00	-37991.59	1.930E+02		
	40.02	0.40	653.98	3.00	-37802.56	1.930E+02		
	40.02	0.40	678.15	3.00	-37843.26	1.930E+02		

	40.02	0.40	706.48	3.00	-37798.62	1.930E+02		
	40.02	0.40	729.82	3.00	-37840.63	1.930E+02		
	40.02	0.40	783.15	3.00	-37677.85	1.930E+02		
FCC	6.00	0.06	627.29	3.00	-65657.06	1.930E+02		
	6.00	0.06	638.17	3.00	-66304.76	1.930E+02		
	6.00	0.06	662.46	3.00	-66648.60	1.930E+02		
	6.00	0.06	678.37	3.00	-67142.59	1.930E+02		
	6.00	0.06	702.66	3.00	-67645.46	1.930E+02		
	6.00	0.06	717.73	3.00	-67979.53	1.930E+02		
	6.00	0.06	730.28	3.00	-68788.04	1.930E+02		
	6.00	0.06	740.33	3.00	-68957.74	1.930E+02		
	6.00	0.06	762.95	3.00	-68981.73	1.930E+02		
	6.00	0.06	781.35	3.00	-70114.53	1.930E+02		
	6.00	0.06	812.33	3.00	-71260.67	1.930E+02		
	6.00	0.06	846.63	3.00	-73046.50	1.930E+02		
	6.60	0.07	627.36	3.00	-63430.54	1.930E+02		
	6.60	0.07	638.24	3.00	-63919.20	1.930E+02		
	6.60	0.07	663.36	3.00	-64582.00	1.930E+02		
	6.60	0.07	678.44	3.00	-64757.03	1.930E+02		
	6.60	0.07	703.56	3.00	-65419.84	1.930E+02		
	6.60	0.07	717.79	3.00	-65912.05	1.930E+02		
	6.60	0.07	740.39	3.00	-66890.26	1.930E+02		
	6.60	0.07	763.01	3.00	-67073.29	1.930E+02		
	6.60	0.07	780.59	3.00	-67728.09	1.930E+02		
	6.60	0.07	813.24	3.00	-68557.93	1.930E+02		
	9.04	0.09	628.27	3.00	-61045.88	1.930E+02		
	9.04	0.09	638.31	3.00	-61374.61	1.930E+02		
	9.04	0.09	664.28	3.00	-61720.23	1.930E+02		
	9.04	0.09	679.35	3.00	-62213.33	1.930E+02		
	9.04	0.09	703.65	3.00	-62398.14	1.930E+02		
	9.04	0.09	718.72	3.00	-62732.20	1.930E+02		
	9.04	0.09	729.59	3.00	-63538.94	1.930E+02		
	9.04	0.09	739.64	3.00	-63867.67	1.930E+02		
	9.04	0.09	762.27	3.00	-63573.59	1.930E+02		
	9.04	0.09	780.67	3.00	-64865.43	1.930E+02		
	9.04	0.09	813.32	3.00	-65854.30	1.930E+02		

	9.04	0.09	845.97	3.00	-67002.21	1.930E+02		
	15.50	0.16	626.82	3.00	-53092.26	1.930E+02		
	15.50	0.16	639.39	3.00	-52946.55	1.930E+02		
	15.50	0.16	653.62	3.00	-53756.84	1.930E+02		
	15.50	0.16	663.68	3.00	-53449.42	1.930E+02		
	15.50	0.16	693.84	3.00	-53799.48	1.930E+02		
	15.50	0.16	713.11	3.00	-53978.95	1.930E+02		
	15.50	0.16	730.68	3.00	-54951.83	1.930E+02		
	15.50	0.16	749.11	3.00	-55130.42	1.930E+02		
	15.50	0.16	777.58	3.00	-55796.77	1.930E+02		
	15.50	0.16	793.49	3.00	-56131.73	1.930E+02		
	15.50	0.16	818.61	3.00	-56794.53	1.930E+02		
	21.93	0.22	683.97	3.00	-47268.31	1.930E+02		
	21.93	0.22	694.86	3.00	-47597.93	1.930E+02		
	21.93	0.22	708.25	3.00	-48089.26	1.930E+02		
	21.93	0.22	717.48	3.00	-47780.96	1.930E+02		
	21.93	0.22	724.17	3.00	-48106.14	1.930E+02		
	21.93	0.22	749.29	3.00	-48768.94	1.930E+02		
	21.93	0.22	763.52	3.00	-49420.19	1.930E+02		
	21.93	0.22	798.68	3.00	-50411.73	1.930E+02		
	21.93	0.22	833.01	3.00	-51561.42	1.930E+02		
Phase	at% Mg	at% ΔMg	Temp (K)	ΔTemp (K)	H (J/mol)	ΔH (J/mol)	Weight	References
B2_BCC	39.00	0.10	273.15	0.50	-16568.64	3.766E+02	1	Robinson *et al.* [33]
	43.90	0.10	273.15	0.50	-17698.32	8.368E+01		
	45.80	0.10	273.15	0.50	-18116.72	8.368E+01		
	49.00	0.10	273.15	0.50	-18367.76	8.368E+01		
	50.30	0.10	273.15	0.50	-18284.08	1.255E+02	0.05	
	51.50	0.10	273.15	0.50	-18367.76	1.255E+02		
	52.00	0.10	273.15	0.50	-18242.24	4.184E+01		
	54.80	0.10	273.15	0.50	-17907.52	8.368E+01		
B2_BCC	50.10	0.10	273.00	1.00	-18744.32	2.092E+02	0.1	Jena *et al.* [35]
	50.10	0.10	195.00	1.00	-18618.80	2.092E+02		
	50.10	0.10	78.00	1.00	-17907.52	2.092E+02		
Phase	at% Mg	at% ΔMg	Temp (K)	ΔTemp (K)	Mur (J/mol)	ΔMur (J/mol)	Weight	References
B2_BCC	42.00	0.04	873.15	3.00	-39655.47	9.649E+01	0.1	Trzebiatowski *et al.*

	44.00	0.04	873.15	3.00	-37436.31	9.649E+01		[32]
	45.50	0.05	873.15	3.00	-38188.90	9.649E+01		
	47.00	0.05	873.15	3.00	-36297.78	9.649E+01		
	48.10	0.05	873.15	3.00	-35603.09	9.649E+01		
	49.30	0.05	873.15	3.00	-32959.39	9.649E+01		
	50.50	0.05	873.15	3.00	-32399.78	9.649E+01		
	51.30	0.05	873.15	3.00	-31975.24	9.649E+01	0.01	
	51.70	0.05	873.15	3.00	-31898.05	9.649E+01		
	52.40	0.05	873.15	3.00	-30836.71	9.649E+01		
	54.20	0.05	873.15	3.00	-29331.54	9.649E+01		
	56.70	0.06	873.15	3.00	-27787.78	9.649E+01		
	57.40	0.06	873.15	3.00	-27710.59	9.649E+01		
	61.10	0.06	873.15	3.00	-25915.96	9.649E+01		
Phase	at% Mg	at% ΔMg	Temp (K)	ΔTemp (K)	H (J/mol)	ΔH (J/mol)	Weight	References
FCC	8.85	0.28	273.15	1.00	-4311.00	1.180E+02	1	Gangulee *et al.* [34]
	8.85	0.28	273.15	1.00	-4429.27	1.180E+02		
	8.85	0.28	273.15	1.00	-4577.12	1.180E+02		
	15.99	0.28	273.15	1.00	-7748.03	1.180E+02		

Appendix II

Let us examine a case where the Gibbs energy models for liquid and β phases are described as follows:

$$G^{\mathrm{L}} = (1 - x_2^{\mathrm{L}})G_1^{\mathrm{RS}\to\mathrm{L}} + x_2^{\mathrm{L}}G_2^{\mathrm{RS}\to\mathrm{L}} + RT(x_2^{\mathrm{L}}\ln x_2^{\mathrm{L}} + (1 - x_2^{\mathrm{L}})\ln(1 - x_2^{\mathrm{L}})) + x_2^{\mathrm{L}}(1 - x_2^{\mathrm{L}}) \times A, \quad (\mathrm{II}\text{-}1)$$

$$G^{\beta} = (1 - x_2^{\beta})G_1^{\mathrm{RS}\to\beta} + x_2^{\beta}G_2^{\mathrm{RS}\to\beta} + RT(x_2^{\beta}\ln x_2^{\beta} + (1 - x_2^{\beta})\ln(1 - x_2^{\beta})) + x_2^{\beta}(1 - x_2^{\beta}) \times B. \quad (\mathrm{II}\text{-}2)$$

Then Eqs. (4.2) and (4.3) can be derived into:

$$G_1^{\mathrm{RS}\to\beta} + RT\ln(1-x_2^{\beta}) + x_2^{\beta}\times B = G_1^{\mathrm{RS}\to\mathrm{L}} + RT\ln(1-x_2^{\mathrm{L}}) + x_2^{\mathrm{L}}\times A, \qquad (\text{II-3})$$

$$G_2^{\mathrm{RS}\to\beta} + RT\ln x_2^{\beta} + (1-x_2^{\beta})\times B = G_2^{\mathrm{RS}\to\mathrm{L}} + RT\ln x_2^{\mathrm{L}} + (1-x_2^{\mathrm{L}})\times A. \qquad (\text{II-4})$$

Calculate x_2^{β} firstly by solving the two equations above, and we have:

$$x_2^{\beta} = \frac{1}{2}\left(1-\sqrt{1-4\exp\left(\frac{G_1^{\mathrm{RS}\to\mathrm{L}} + G_2^{\mathrm{RS}\to\mathrm{L}} + RT\ln x_2^{\mathrm{L}}(1-x_2^{\mathrm{L}}) + A - G_1^{\mathrm{RS}\to\beta} - G_2^{\mathrm{RS}\to\beta} - B}{RT}\right)}\right) (\text{II-5})$$

or

$$x_2^{\beta} = \frac{1}{2}\left(1+\sqrt{1-4\exp\left(\frac{G_1^{\mathrm{RS}\to\mathrm{L}} + G_2^{\mathrm{RS}\to\mathrm{L}} + RT\ln x_2^{\mathrm{L}}(1-x_2^{\mathrm{L}}) + A - G_1^{\mathrm{RS}\to\beta} - G_2^{\mathrm{RS}\to\beta} - B}{RT}\right)}\right) (\text{II-6})$$

Apparently, x_2^{β} is non-linear to parameters A and B. T can be obtained by substituting x_2^{β} into Eq. (II-4), then we have:

$$T = \frac{G_2^{\mathrm{RS}\to\mathrm{L}} - G_2^{\mathrm{RS}\to\beta} + (1-x_2^{\mathrm{L}})\cdot A - (1-x_2^{\beta})\times B}{R\ln\dfrac{x_2^{\beta}}{x_2^{\mathrm{L}}}}, \qquad (\text{II-7})$$

which must be non-linear to parameters A and B as well as x_2^{β} is non-linear to parameters A and B.

Appendix III

Phase	Thermodynamic parameters of the model (J/mol)	Reference
Liquid	$(\mathrm{Ag, Mg})$ ${}^{0}L^{\mathrm{Liq}}_{\mathrm{Ag,Mg}} = -50999.87 - 13.09T$ ${}^{1}L^{\mathrm{Liq}}_{\mathrm{Ag,Mg}} = -3999.69$	This work
$\mathrm{AgMg_3}$	$(\mathrm{Ag})_{0.23}(\mathrm{Mg})_{0.77}$ ${}^{0}G^{\mathrm{AgMg3}}_{\mathrm{Ag:Mg}} = 0.23\,{}^{298}H^{\mathrm{FCC\_A1}}_{\mathrm{Ag}} + 0.77\,{}^{298}H^{\mathrm{HCP\_A3}}_{\mathrm{Mg}} - 21600 + 12.8T$	Lim *et al.*[21]
$\mathrm{AgMg_4}$	$(\mathrm{Ag})_{0.2}(\mathrm{Mg})_{0.8}$ ${}^{0}G^{\mathrm{AgMg4}}_{\mathrm{Ag:Mg}} = 0.2\,{}^{298}H^{\mathrm{FCC\_A1}}_{\mathrm{Ag}} + 0.8\,{}^{298}H^{\mathrm{HCP\_A3}}_{\mathrm{Mg}} - 20458 + 13.36T$	Lim *et al.*[21]
B2_BCC	$(\mathrm{Ag, Mg})_1\,\mathrm{Va}_3$ ${}^{0}L^{\mathrm{B2\_BCC}}_{\mathrm{Ag,Mg}} = -29454.82 - 28.88T$ ${}^{1}L^{\mathrm{B2\_BCC}}_{\mathrm{Ag,Mg}} = -34253.87 + 29.29T$ ${}^{3}L^{\mathrm{B2\_BCC}}_{\mathrm{Ag,Mg}} = 33400 - 59.99T$	This work
	$(\mathrm{Ag,Mg})_{0.5}(\mathrm{Ag,Mg})_{0.5}\mathrm{Va}_1$ ${}^{0}G^{\mathrm{B2\_BCC}}_{\mathrm{Ag:Mg}} = -32152.29 + 13.22T$ ${}^{0}G^{\mathrm{B2\_BCC}}_{\mathrm{Mg:Ag}} = -32152.29 + 13.22T$	This work
FCC	$(\mathrm{Ag, Mg})_1\,\mathrm{Va}_1$ ${}^{0}L^{\mathrm{FCC}}_{\mathrm{Ag,Mg}} = -59997.86$ ${}^{1}L^{\mathrm{FCC}}_{\mathrm{Ag,Mg}} = 17194.59 - 30.84T$ ${}^{3}L^{\mathrm{FCC}}_{\mathrm{Ag,Mg}} = 9T$	This work
$\mathrm{L1_2}$ (first-order)	$(\mathrm{Ag,Mg})_{0.25}(\mathrm{Ag,Mg})_{0.25}\,(\mathrm{Ag,Mg})_{0.25}(\mathrm{Ag,Mg})_{0.25}\mathrm{Va}_1$ ${}^{0}G^{\mathrm{L12}}_{\mathrm{Ag:Ag:Ag:Mg}} = {}^{0}G^{\mathrm{L12}}_{\mathrm{Ag:Ag:Mg:Ag}} = {}^{0}G^{\mathrm{L12}}_{\mathrm{Ag:Mg:Ag:Ag}} = {}^{0}G^{\mathrm{L12}}_{\mathrm{Mg:Ag:Ag:Ag}} = -9971.51$ ${}^{0}G^{\mathrm{L12}}_{\mathrm{Ag:Ag:Mg:Mg}} = {}^{0}G^{\mathrm{L12}}_{\mathrm{Ag:Mg:Mg:Ag}} = {}^{0}G^{\mathrm{L12}}_{\mathrm{Ag:Mg:Ag:Mg}}$ $= {}^{0}G^{\mathrm{L12}}_{\mathrm{Mg:Ag:Ag:Mg}} = {}^{0}G^{\mathrm{L12}}_{\mathrm{Mg:Ag:Mg:Ag}} = {}^{0}G^{\mathrm{L12}}_{\mathrm{Mg:Mg:Ag:Ag}} = -6647.6711$ ${}^{0}G^{\mathrm{L12}}_{\mathrm{Mg:Mg:Mg:Ag}} = {}^{0}G^{\mathrm{L12}}_{\mathrm{Mg:Mg:Ag:Mg}} = {}^{0}G^{\mathrm{L12}}_{\mathrm{Mg:Ag:Ag:Ag}} = {}^{0}G^{\mathrm{L12}}_{\mathrm{Ag:Mg:Mg:Mg}} = -9971.51$	This work
$\mathrm{L1_2}$ (second-order)	$(\mathrm{Ag,Mg})_{0.5}(\mathrm{Ag,Mg})_{0.5}\mathrm{Va}_1$	This work

	$^{0}G^{\mathrm{L12}}_{\mathrm{Ag:Mg}} = -7290$ $^{0}G^{\mathrm{L12}}_{\mathrm{Mg:Ag}} = -7290$	
HCP_A3	$(\mathrm{Ag},\mathrm{Mg})_1\mathrm{Va}_{0.5}$ $^{0}L^{\mathrm{HCP\_A3}}_{\mathrm{Ag,Mg}} = -22618 - 14.63T$	Lim *et al.*[21]

Appendix IV

The interval approach has been implemented in MATLAB, and its GUI (graphical user interface) is shown in Figure IV-1.

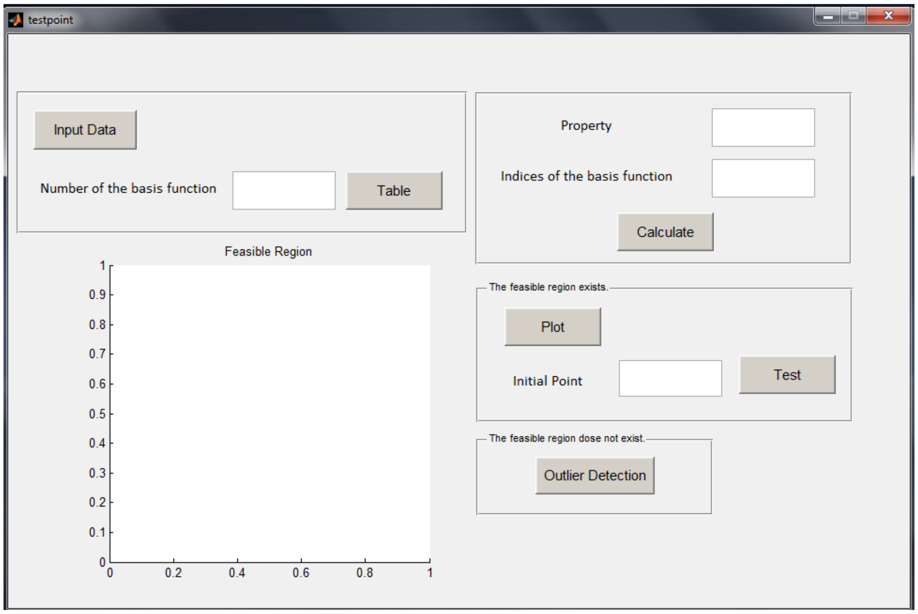

Figure IV-1: The graphical user interface.

The program starts with clicking the button ***Input Data***, and we use the data from Kawakami [20] as an example, which is reported in Table IV-1.

Table IV-1: Input data

x_{Mg}	T (K)	${}^{\mathrm{mix}}H^{\mathrm{Liq}}_{\mathrm{AgMg}}$ (J/mol) Upper	${}^{\mathrm{mix}}H^{\mathrm{Liq}}_{\mathrm{AgMg}}$ (J/mol) lower
0.2514	1323	-7140.4	-9697.06
0.295	1323	-10266.8	-13123.7
0.4192	1323	-11085.3	-14051.8
0.5341	1323	-11436.5	-14462.9
0.5425	1323	-10851.5	-13650.8
0.5748	1323	-11150.9	-13851.2
0.6461	1323	-9631.76	-12086.6
0.7225	1323	-9146.71	-11507.1
0.7368	1323	-7346.75	-9472.39
0.8403	1323	-6408.44	-8188.57

For the present program, the Redlich – Kister formalism (i.e., Eq. (3.2)) is chosen as the default Gibbs energy model that can be composition and temperature dependent. The basis function is a table of available parameters of the model, and the number indicates the number of rows of the table (The table is shown in Figure IV-2).

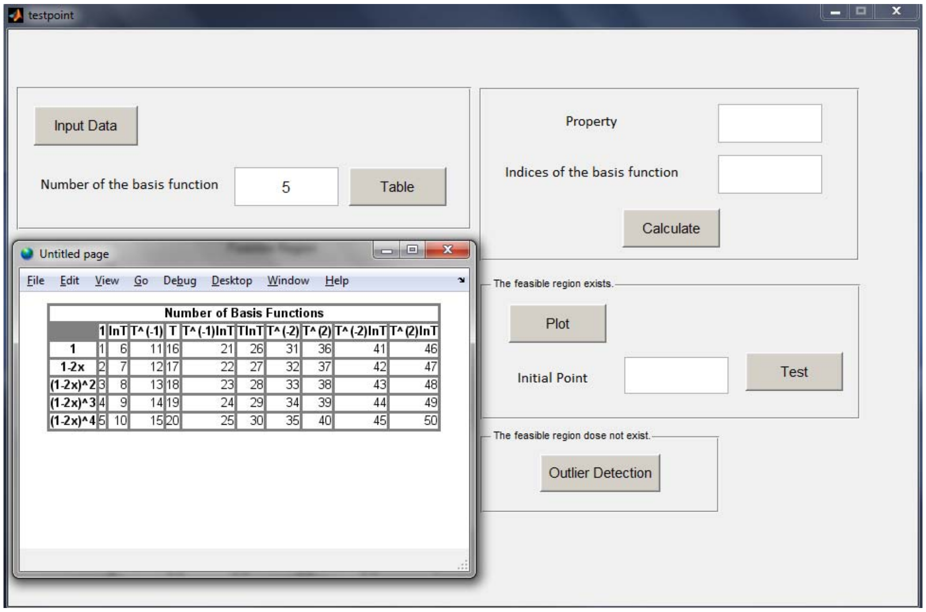

Number of the basis function 5

Number of Basis Functions

	1	lnT	T^(-1)	T	T^(-1)lnT	TlnT	T^(-2)	T^(2)	T^(-2)lnT	T^(2)lnT
1	1	6	11	16	21	26	31	36	41	46
1-2x	2	7	12	17	22	27	32	37	42	47
(1-2x)^2	3	8	13	18	23	28	33	38	43	48
(1-2x)^3	4	9	14	19	24	29	34	39	44	49
(1-2x)^4	5	10	15	20	25	30	35	40	45	50

Figure IV-2: A table of available parameters, when the number of the basis function is 5.

According to the definition of the program, ***H*** stands for the mixing enthalpy that corresponds to the property of the input. The next step is to determine the exact Gibbs energy model by choosing the numbers from the table of basis functions. As we are interested in a sub-regular model (i.e., Eq. (7.10)), the numbers 1 and 2 are chosen (Figure IV-3).

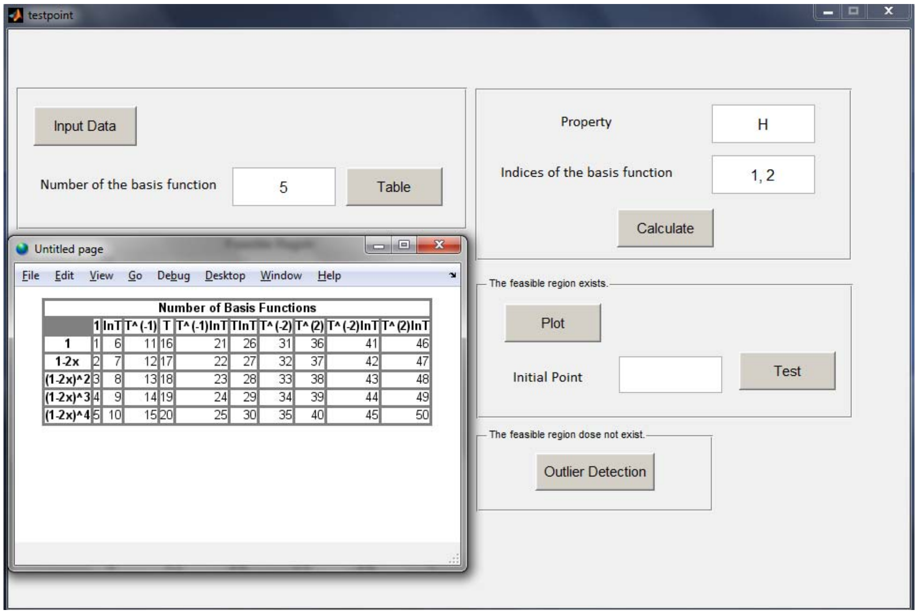

Number of the basis function: 5

Property: H

Indices of the basis function: 1, 2

Number of Basis Functions										
	1	lnT	T^(-1)	T	T^(-1)lnT	TlnT	T^(-2)	T^(2)	T^(-2)lnT	T^(2)lnT
1	1	6	11	16	21	26	31	36	41	46
1-2x	2	7	12	17	22	27	32	37	42	47
(1-2x)^2	3	8	13	18	23	28	33	38	43	48
(1-2x)^3	4	9	14	19	24	29	34	39	44	49
(1-2x)^4	5	10	15	20	25	30	35	40	45	50

Figure IV-3: A sub-regular model is determined by selecting the numbers 1 and 2 from the table of basis functions.

Click the button ***Calculate*** and you will receive a message that tells you whether or not a feasible region exists (Figure IV-4). In the present case, we have obtained a feasible region.

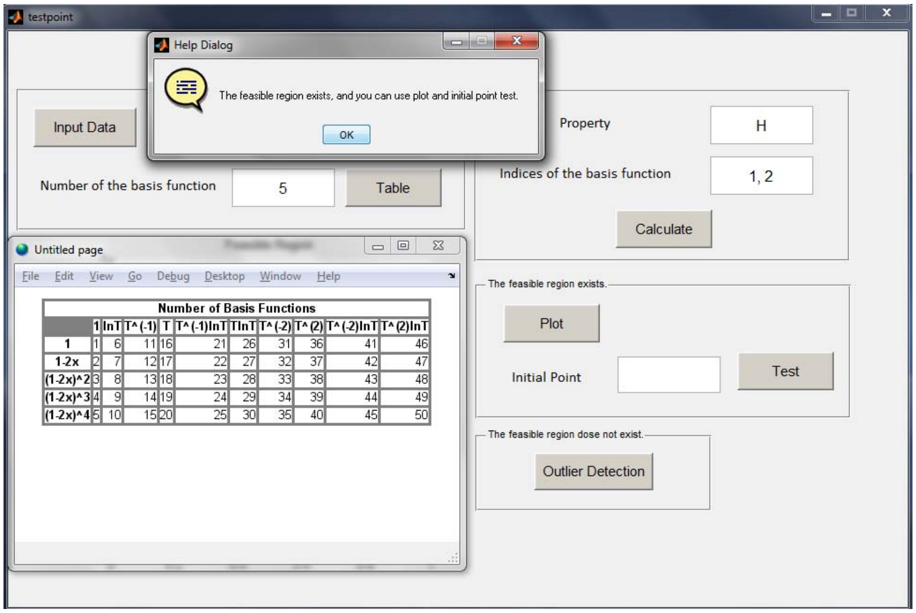

The feasible region exists, and you can use plot and initial point test.

Number of the basis function: 5

Property: H

Indices of the basis function: 1, 2

Number of Basis Functions										
	1	lnT	T^(-1)	T	T^(-1)lnT	TlnT	T^(-2)	T^(2)	T^(-2)lnT	T^(2)lnT
1	1	6	11	16	21	26	31	36	41	46
1-2x	2	7	12	17	22	27	32	37	42	47
(1-2x)^2	3	8	13	18	23	28	33	38	43	48
(1-2x)^3	4	9	14	19	24	29	34	39	44	49
(1-2x)^4	5	10	15	20	25	30	35	40	45	50

Figure IV-4: A message from the program: the feasible region exists.

Then we can plot this feasible region on the screen (Figure IV-5), where parameters a and b respectively stand for the parameters A_0 and A_1 of Eq. (7.10).

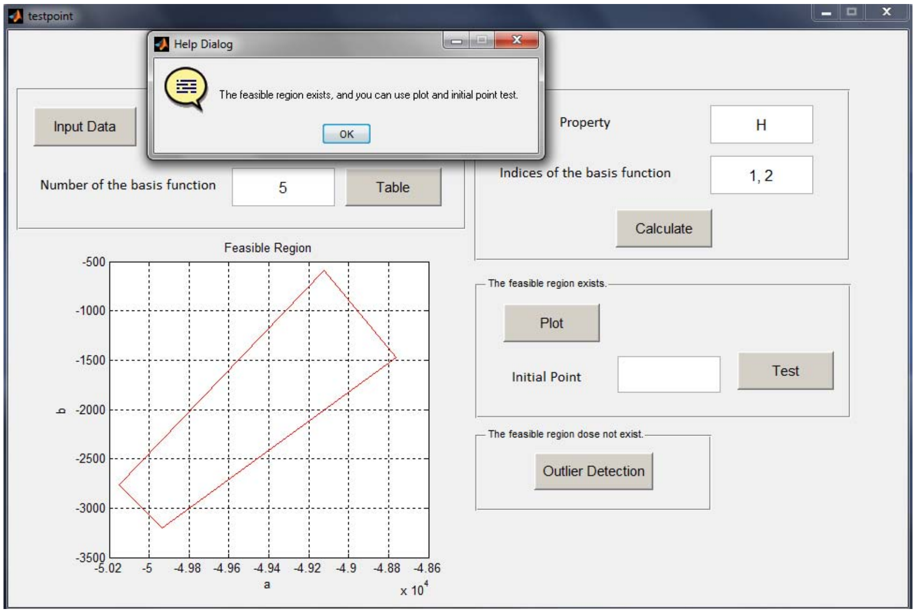

The feasible region exists, and you can use plot and initial point test.

Number of the basis function: 5

Property: H

Indices of the basis function: 1, 2

Initial Point:

Figure IV-5: Plot the feasible region.

The program has a particular feature that can identify whether a point belongs to the feasible region. Moreover, it would save much time to find satisfactory initial values of parameters by using this method.

Figure IV-6 shows a case where A_0=-49000 and A_1=-1500. After the test, this set of parameters was confirmed to belong to the feasible region.

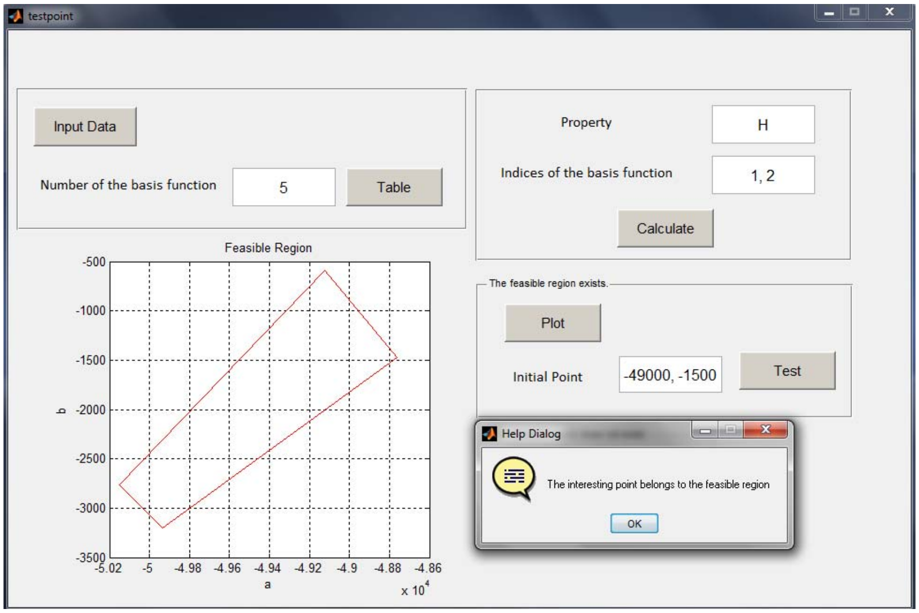

Number of the basis function 5

Property H

Indices of the basis function 1, 2

The feasible region exists.

Initial Point -49000, -1500

The interesting point belongs to the feasible region

Figure IV-6: Test a point whether or not belongs to the feasible region, where A_0=-49000 and A_1=-1500.

Figure IV-7 shows a case where A_0=-49000 and A_1=-3500, and this point does not belong to the feasible region after the test.

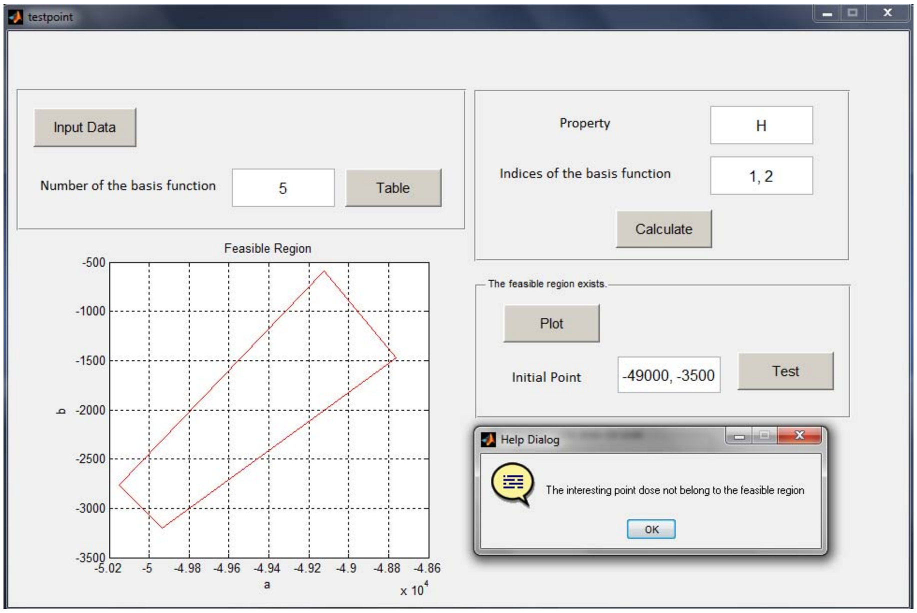

Number of the basis function: 5

Property: H

Indices of the basis function: 1, 2

The feasible region exists.

Initial Point: -49000, -3500

The interesting point dose not belong to the feasible region

Figure IV-7: Test a point whether or not belongs to the feasible region, where A_0=-49000 and A_1=-3500.

Reference List

1. S. K. Choudhary, ISIJ International **51,** 557 (2011).

2. Chuck Fryman. Clean-Steel Practices in the Melt Shop. Industrial Heating Magazine . 2011.

Ref Type: Magazine Article

3. Z. Deng and M. Zhu, steel research int. **84,** 519 (2013).

4. D. H. Herring, Industrial Heating **76,** 18,20 (2009).

5. Z. h. JIANG, S. j. LI, and Y. LI, Journal of Iron and Steel Research, International **18,** 14 (2011).

6. H. Suito and R. Inoue, ISIJ International **36,** 528 (1996).

7. H. Todoroki and K. Mizuno, ISIJ International **44,** 1350 (2004).

8. K.Mizuno, H.Todoroki, M.Noda, and T.Tohge. ISS Transactions, Iron Steelmaker 28[8], 93. 2001.

Ref Type: Magazine Article

9. P. Kaushik, M. Lowry, H. Yin, and H. Pielet, Ironmaking & Steelmaking **39,** 284 (2012).

10. H.Todoroki, K.Mizuno, M.Noda, and T.Tohge. Steelmaking Conf.Proc. 84, 331. 2001.

Ref Type: Magazine Article

11. H.Todoroki and S.Inada. Bull.Iron Steel Inst.Jpn. 8, 575. 2003.

Ref Type: Magazine Article

12. Jimmy Gran, Minho Song, and Du Sichen, Calphad **36,** 89 (2012).

13. H. Fujiwara, M. Tano, K. Yamamoto, and E. Ichise, ISIJ International **35,** 1063 (1995).

14. J. Chipman and T. P. Floridis, Acta Metallurgica **3,** 456 (1955).

15. C. L. Nassaralla and E. T. Turkdogan, MTB **24,** 963 (1993).

16. A.T.Dinsdale, Calphad **15,** 317 (1991).

17. Thermo-Calc Software A.B., *Thermo-Calc Database Guide* (Stockholm Technology Park, Stockholm, 2006).

18. P.Spencer, Calphad **32,** 1 (2008).

19. A.A.Nayeb-Hashemi and J.B.Clark, Bulletin of Alloy Phase Diagram **5,** 348 (1984).

20. M.Kawakami, Sci. Rep. Res. Inst. Tohoku Univ. **7,** 351 (1930).

21. Michael Lim, John E.Tibballs, and Paul L.Rossiter, Zeitschrift fur Metallkunde **88,** 162 (1997).

22. W.Hume-Rothery and E.Butchers, J. Jpn. Ins. Met. **60,** 345 (1937).

23. S.F.Zemczuznyj, Zeitschrift fur Metallkunde **49,** 400 (1906).

24. R.J.M.Payne and J.L.Haughton, J. Jpn. Ins. Met. **60,** 351 (1937).

25. K.W.Andrews and W.Hume-Rothery, J. Jpn. Ins. Met. **69,** 485 (1943).

26. E.Schuermann and R.Engel, Giessereiforschung **32,** 58 (1986).

27. V.E.Kolesnichenko, V.V.Karonik, and S.N.Tsyganova, Izvestiya Akademii Nauk SSSR. Metally **5,** 186 (1988).

28. P.Schubel, Z. Anorg. Chem. **87,** 81 (1914).

29. Sukeji Kachi, Sci. Rep. Res. Inst. Tohoku Univ. **A7,** 351 (1955).

30. Kunio Fujiwara, Makoto Hirabayashi, Denjiro Watanabe, and Shiro Ogawa, J. Jpn. Ins. Met. **12,** 167 (1958).

31. B.A.Buckley, H.J.Axon, and J.Conacher, Journal of the Institute of Metals **88,** 225 (1960).

32. W.Trzebiatowski and J.Terpilowski, Bull. Acad. Pol. Sci. **3,** 391 (1955).

33. P.M.Robinson and M.B.Bever, Trans. Met. Soc. AIME **230,** 1487 (1964).

34. A.Gangulee and M.B.Bever, Trans. Met. Soc. AIME **242,** 277 (1968).

35. A.K.Jena and M.B.Bever, Trans. Met. Soc. AIME **242,** 2369 (1968).

36. M. Hamalainen, E. Laine, and T. Tarna, J. Appl. Cryst. **2,** 95 (1969).

37. J.Kulik, S.Takeda, and D.de Fontaine, Acta Metallurgica **35,** 1137 (1987).

38. A. Gangulee and S. C. Moss, J. Appl. Cryst. **1,** 61 (1968).

39. Y.Fujino, Phys. Rev. B **42,** 5373 (1990).

40. Otto Redlich and A.T.Kister, Industrial Engineering Chemistry **40,** 345 (1948).

41. M.Hillert. and L.I.Staffansson, Acta Chemica Scandinavica **24,** 3618 (1970).

42. H.L.Lukas, S.G.Fries, and B.Sundman, *Computational thermodynamics, the calphad method* (Cambridge university press, United Kingdom, 2007).

43. I. Ansara, N. Dupin, H. L. Lukas, and B. Sundman, Journal of Alloys and Compounds **247,** 20 (1997).

44. Bo Jansson, Ph. D. Thesis, Division of Physical Metallurgy, Royal Inst. Of Technology, 1984.

45. Thermo-Calc Software AB. [S]. 2008.

Ref Type: Computer Program

46. R. G. Jordan *et al.*, Phys. Rev. B **50,** 11459 (1994).

47. L.V.Kantorovich, Siberian Mathematical Journal **3,** 701 (1962).

48. J.Rohn and V.Kreinovich, SIAM Journal on MatrixAnalysis and Applications **16,** 415 (1995).

49. Eric Walter and Helene Piet-Lahanier, Mathematics and Computers in Simulation **32,** 449 (1990).

50. G.B.Dantzig, A.Orden, and P.Wolfe, Pacific Journal Math. **5,** 183 (1955).

51. G.Belforte, B.Bona, and V.Cerone, in *Parameter estimation with set membership uncertainty: nonlinear families of models*, 1988), p. 399.

52. E.Walter, H.Piet-Lahanier, and J.Happel, Math. Comput. Simulation **28,** 479 (1986).

53. Kim Bartke, in *2D, 3D and High-Dimensional Data and Information Visualization*, University of Hannover, 2005).

54. Inderjit S., Dharmendra S.Modha, and W.Scott Spangler, Computational Statistics & Data Analysis **41,** 59 (2002).

55. S.I.Zhilin, Reliable Computing **11,** 433 (2005).

56. S.I.Zhilin, Chemometrics and Intelligent Laboratory Systems **88,** 60 (2007).

57. S.I.Spivak, M.G.Slinko, V.I.Timoshenko, and V.Yu.Mashkin, Reaction Kinetics and Catalysis Letters **3,** 105 (1975).

58. A.Pomerantsev and O.Rodionova, Journal of Analytical Chemistry **61,** 925 (2006).

59. O.Rodionova and A.Pomerantsev, Chemometrics and Intelligent Laboratory Systems **97,** 64 (2009).

60. O.Rodionova and A.Pomerantsev, Russian Chemical Reviews **75,** 271 (2006).

61. O.Rodionova, K.Esbensen, and A.Pomerantsev, Journal of Chemometrics **18,** 402 (2004).